AGU ADVANCING EARTH AND SPACE SCIENCE

JGR Atmospheres

RESEARCH ARTICLE
10.1029/2022JD036957

Key Points:

- The cloud scattering lookup tables of Community Radiative Transfer Model (CRTM) discussed and documented
- A new scattering database generated using the Discrete Dipole Approximation (DDA) implemented into CRTM
- The scattering parameters computed using the DDA technique perform considerably better than Mie coefficients for microwave frequencies

Correspondence to:
I. Moradi,
imoradi@umd.edu

Citation:
Moradi, I., Stegmann, P., Johnson, B., Barlakas, V., Eriksson, P., Geer, A., et al. (2022). Implementation of a discrete dipole approximation scattering database into community radiative transfer model. *Journal of Geophysical Research: Atmospheres*, *127*, e2022JD036957. https://doi.org/10.1029/2022JD036957

Received 16 APR 2022
Accepted 1 DEC 2022

Author Contributions:
Conceptualization: Isaac Moradi
Data curation: Isaac Moradi
Formal analysis: Isaac Moradi
Funding acquisition: Isaac Moradi
Investigation: Isaac Moradi
Methodology: Isaac Moradi
Project Administration: Isaac Moradi
Resources: Isaac Moradi
Software: Isaac Moradi
Supervision: Isaac Moradi
Validation: Isaac Moradi
Visualization: Isaac Moradi
Writing – original draft: Isaac Moradi

Implementation of a Discrete Dipole Approximation Scattering Database Into Community Radiative Transfer Model

Isaac Moradi[1,2,3], Patrick Stegmann[4], Benjamin Johnson[4], Vasileios Barlakas[5], Patrick Eriksson[5], Alan Geer[6], Ronald Gelaro[3], Satya Kalluri[7], Daryl Kleist[8], Quanhua Liu[9], and Will Mccarty[10]

[1]Earth System Science Interdisciplinary Center (ESSIC), University of Maryland, College Park, MD, USA, [2]Cooperative Institute for Satellite Earth System Studies (CISESS), University of Maryland, College Park, MD, USA, [3]NASA Global Modeling and Assimilation Office, Greenbelt, MD, USA, [4]Joint Center for Satellite Data Assimilation, UCAR, Boulder, CO, USA, [5]Department of Space, Earth and Environment, Chalmers University of Technology, Gothenburg, Sweden, [6]European Centre for Medium-Range Weather Forecasts, Shinfield Park, Reading, UK, [7]NOAA Joint Polar Satellite System (JPSS) Program Science Office, Lanham, MD, USA, [8]NOAA National Centers for Environmental Prediction, Environmental Modeling Center, College Park, MD, USA, [9]NOAA Center for Satellite Applications and Research, College Park, MD, USA, [10]NASA Headquarters, Washington, DC, USA

Abstract The Community Radiative Transfer Model (CRTM) is a fast model that requires bulk optical properties of hydrometeors in the form of lookup tables to simulate all-sky satellite radiances. Current cloud scattering lookup tables of CRTM were generated using the Mie-Lorenz theory thus assuming spherical shapes for all frozen habits, while actual clouds contain frozen hydrometeors with different shapes. The Discrete Dipole Approximation (DDA) technique is an effective technique for simulating the optical properties of non-spherical hydrometeors in the microwave region. This paper discusses the implementation and validation of a comprehensive DDA cloud scattering database into CRTM for the microwave frequencies. The original DDA database assumes total random orientation in the calculation of single scattering properties. The mass scattering parameters required by CRTM were then computed from single scattering properties and water content dependent particle size distributions. The new lookup tables eliminate the requirement for providing the effective radius as input to CRTM by using the cloud water content for the mass dimension. A collocated dataset of short-term forecasts from Integrated Forecast System of the European Center for Medium-Range Weather Forecasts and satellite microwave data was used for the evaluation of results. The results overall showed that the DDA lookup tables, in comparison with the Mie tables, greatly reduce the differences among simulated and observed values. The Mie lookup tables especially introduce excessive scattering for the channels operating below 90 GHz and low scattering for the channels above 90 GHz.

Plain Language Summary Radiative transfer (RT) models have a wide range of applications in remote sensing, satellite data calibration, instrument design, and weather forecasts. Although, the clear-sky simulations conducted by the RT models are relatively accurate, the accuracy of these models for simulating all-sky observations remains limited. One of the main reasons for inaccuracies in all-sky simulations is known to be the scattering databases used to calculate the optical properties of different cloud hydrometeors. We implemented and evaluated a large scattering database, computed using the Discrete Dipole Approximation (DDA) technique, into the Community Radiative Transfer Model (CRTM). The results showed that the simulations conducted using the DDA database are much more accurate than the corresponding simulations conducted using the Mie scattering lookup tables which assumes spherical particles for all hydrometeors.

1. Introduction

Assimilation of all-sky satellite microwave (MW) observations into Numerical Weather Prediction (NWP) models plays an important role in improving routine weather forecasts as well as prediction of extreme weather events such as tropical cyclones (Duncan et al., 2022). Unlike infrared observations which are normally saturated in the presence of optically thick clouds, MW instruments continue to provide useful information even in the presence of deep convective clouds. Data assimilation systems generally use a fast radiative transfer (RT) model as the forward operator to assimilate satellite observations into the first guess provided by the NWP models (Baordo & Geer, 2016; Geer et al., 2021; Moradi, Evans, et al., 2020).

The Community Radiative Transfer Model (CRTM) is a fast model developed by the NOAA Joint Center for Satellite Data Assimilation (JCSDA) (Liu et al., 2008). CRTM is currently used as the observation operator within the NOAA Finite-Volume Cubed-Sphere Dynamical Core system (Tong et al., 2020), NASA Goddard Earth Observing System (Gelaro et al., 2017; Tong et al., 2020) and the Navy Earth System Prediction Capability (Barton et al., 2021) to enable assimilation of satellite observations into the NWP models. CRTM is also used across the NOAA National Environmental Satellite, Data, and Information Service (NESDIS) for simulating satellite observations for the quality assurance and quality control of measurements from the underlying satellite instruments (Weng et al., 2013). In addition, CRTM is broadly used as forward model in inverse retrieval systems for deriving geophysical variables from satellite measurements (Boukabara et al., 2011). Additionally, several Observing System Simulation Experiment (OSSE) frameworks currently employ CRTM to generate synthetic satellite observations which are used for the design or evaluation of future satellite instruments (Boukabara et al., 2016; McCarty et al., 2021). Although, CRTM clear-sky simulations are reported to have reasonable accuracy in the MW frequencies (Moradi, Goldberg, et al., 2020), accurate simulations of all-sky MW satellite observations is still a challenge for CRTM as well as many other RT models.

In addition to the geophysical variables (e.g., temperature, water vapor, and pressure) and cloud information (water content, effective radius, and cloud type), CRTM requires cloud optical properties for simulating all-sky satellite radiances. In practice, the optical properties of idealized ice and snow particles are precomputed and stored in lookup tables. Current CRTM scattering lookup tables were generated using the Mie-Lorenz theory (hereafter referred to as Mie theory for simplicity) which assumes spherical shapes for both liquid and frozen hydrometeors (Stegmann et al., 2018). Although the optical properties of liquid clouds can be modeled efficiently using the Mie theory by assuming spherical shapes for the hydrometeors (Eriksson et al., 2018), frozen hydrometeors (ice clouds, snow, graupel, and hail) exhibit a large variation in the shape. As a result, all-sky simulations conducted using the lookup tables generated using the Mie theory for the frozen particles largely deviate from the observations (Baordo & Geer, 2016; Eriksson et al., 2015, 2018; Geer & Baordo, 2014). Although CRTM has a good accuracy in simulating clear-sky observations from the input profiles (Moradi, Goldberg, et al., 2020), using Mie theory to generate the scattering lookup tables is known to limit the accuracy of the CRTM all-sky calculations (Sieron et al., 2017).

In order to reduce biases in the all-sky simulations conducted using the Mie lookup tables, it is often necessary to tune other cloud parameters such as size of the particles. These adjustments may improve the results for some channels but most likely increase the bias in the simulations for other channels. RT calculations performed using the Mie lookup tables also tend to produce the worst results over the convective regions causing difficulties for assimilation of MW observations over the rainbands of tropical cyclones (Geer & Baordo, 2014). The forward model error is indeed only one factor limiting the assimilation of all-sky MW observations in NWP, alongside systematic errors in forecast models and the intrinsic lack of predictability of cloud and precipitation. In order to mitigate these large error sources in the all-sky assimilation, the NWP centers rely on mechanism such as inflating the observation error (Geer & Bauer, 2011; Zhu et al., 2015), correcting the observations using the variational bias correction, and excluding the observations when the forward operator is not able to simulate them with enough accuracy (Baordo & Geer, 2016).

The exact solutions to Maxwell equations are only known for particular geometries such as spheres, spheroids, or cylinders, thus approximations are needed to calculate the optical properties of particles with arbitrary shapes. The discrete dipole approximation (DDA) estimates the optical properties of objects in terms of discrete dipoles (DeVoe, 1964). Several scattering lookup tables generated using the DDA technique are available for the MW frequencies including, Liu (2004) (frequencies of 85.5, 150, and 220 GHz), Liu (2008) (frequency range of 15–340 GHz), Hong (2007) (89–340 GHz), Hong et al. (2009) (100–1,000 GHz), and Eriksson et al. (2018) (frequency range of 1–886 GHz). Ding et al. (2017) also generated a dataset for several non-spherical ice particles using the embedded T-matrix method for the frequency range of 1–874 GHz. We selected the database generated by Eriksson et al. (2018) (ARTS) based on the availability of the single scattering data, frequency and temperature range, and also number of shapes used to generate the database. Although we evaluated the Liu (2008) (Liu08) database, this database only provides a few habits that can be used for snow clouds, thus the paper mainly focuses on implementation and validation of the database created by Eriksson et al. (2018). Both ARTS and Liu08 assumes total random orientation in the calculation of single scattering properties, however a newer version of the ARTS database provides the scattering properties for oriented ice particles (Brath et al., 2020). Note that ARTS database includes many habits that may have been used in other datasets, for instance, 8-column

aggregate, solid hexagonal column, hexagonal plate, solid bullet rosette, spheroids, and sphere from the ARTS database are also included in the database developed by Ding et al. (2017).

In addition to the in-depth analysis of the ARTS scattering database, we use a collocated satellite MW and atmospheric dataset to evaluate the results of the CRTM all-sky simulations. Because of lack of documentation for the CRTM cloud coefficient files, bulk parameters stored in the CRTM lookup tables are discussed in great details in this paper to serve as a future guide for generating the scattering lookup tables for CRTM. It should be noted that there is a RT model named Atmospheric Radiative Transfer Simulator (ARTS), however the simulations referred to as ARTS in this paper are the CRTM simulations conducted using the ARTS DDA scattering database.

Section 2 discusses the satellite observations and atmospheric dataset used in the study, Section 3 summarizes the scattering database, Section 4 describes the RT model, Section 5 discusses the bulk optical properties required by CRTM including the new cloud lookup tables generated from the ARTS database, Section 6 discusses the results, and Section 7 summarizes the work.

2. Collocated Atmospheric and Satellite Observations

CRTM requires a set of atmospheric and surface variables including profiles of temperature, water vapor, and pressure, sea surface temperature, as well as surface wind speed and direction in order to simulate the clear-sky brightness temperatures. In addition, profiles of cloud fraction and layer integrated water contents of snow, ice, liquid, rain, hail, and graupel hydrometeors are required to simulate cloud contaminated brightness temperatures. We used the short-term forecasts from the NWP system of European Center for Medium Range Weather Forecast (ECMWF), known as Integrated Forecast System (IFS), as input to CRTM to simulate all-sky brightness temperatures then compared the CRTM simulations with observations from the Advanced Technology Microwave Sounder (ATMS) instrument. We originally used the ERA5 dataset, the fifth generation of the ECMWF atmospheric reanalysis, for the comparison between observed and simulated values, however because of the lack of convective clouds in ERA5, we switched to a comprehensive dataset that was produced using IFS with both convective and large scale clouds included (Geer, 2022).

The dataset was generated using IFS cycle 47r1 from a run of the forecast model with the initial conditions taken from the operational analysis at 00:00 UTC, 7 September 2017 and validity times from 09:00 to 21:00 UTC on that day. The IFS model used a horizontal resolution of T1279co (equivalent to 8–9 km) and 137 hybrid vertical pressure levels with a temporal resolution of 7.5 min, although only every fourth model time-step was available for collocation. Interpolation of atmospheric and surface data to the location of ATMS observations was performed on the fly eliminating the need for later collocations (Geer, 2022). The temporal and horizontal resolutions of the IFS run introduces a time difference of less than 15 min and spatial distance of less than 5 km between observations and the model grid. In addition to the atmospheric profiles and surface information, the IFS run provided profiles of mass mixing ratios of cloud liquid and ice water content as well as convective and large scale rain and snow water contents. These water content values were used to run the CRTM cloudy simulations. It is suggested to use convective snow water content for graupel and large-scale snow water content for snow habits (Geer, 2022). In order to run a full ensemble of clouds, we split the convective snow water content evenly (50% each) between graupel and hail. Because of the similarity between scattering properties of hail and graupel, the difference between CRTM simulations when the convective snow water content is assigned to hail and graupel or only graupel is very small and does not affect the conclusions.

ATMS is the newest generation of MW instruments flown on NOAA satellites with 22 channels operating roughly from 23 to 190 GHz. Some of the ATMS channels which were designed to measure upper troposphere and stratospheric temperature have a weighting function well above the clouds, therefore they have a very low sensitivity to clouds. However, channels 1–8 operating from 23 to 55 GHz are sensitive to liquid clouds, rain, and to a lower extent snow, graupel, and hail and channels 16–22 operating around 90 GHz and above are sensitive to different frozen hydrometeors such as ice clouds, hail, graupel, and snow (Goldberg et al., 2013; Kim et al., 2014; Moradi et al., 2015). The spatial resolution of the ATMS channels depends on both frequency and zenith angle. The ATMS footprint size at nadir is roughly 75 km for channels 1–2, 32 km for channels 3–16, and 16 km for channels 17–22. However, the ATMS footprint size increases with the zenith angle so that at the edge of the scan-lines with a zenith angle of about 62°, it translates to 323 km for channels 1–2, 136 km for channels 3–16, and 68 km for channels 17–22 in cross-track direction (Kim et al., 2014).

3. Scattering Databases

3.1. CRTM Cloud Coefficients

Current CRTM cloud coefficient files include mass extinction coefficient (m^2 kg^{-1}), single scatter albedo (unitless), asymmetry parameter (unitless), and the phase function in terms of Legendre coefficients. The scattering parameters are separately provided for liquid and frozen hydrometeors in the CRTM cloud coefficients (note that we use the terms *cloud* and *hydrometeor* interchangeably throughout the paper). In the current coefficient files, these parameters are given as a function of temperature, effective radius, and frequency for liquid phase but only as a function of effective radius and frequency for frozen particles. The current scattering coefficients of CRTM are not well documented, but Stegmann et al. (2018) provides a good overview of the current status of the CRTM cloud coefficients.

The same scattering parameters are used for both water (`WATER_CLOUD`) and rain (`RAIN_CLOUD`) hydrometeors. The difference between rain and water clouds is that in the case of `WATER_CLOUD`, the extinction coefficients of the first bin of effective radius in the lookup tables are extracted then interpolated as a function of frequency and temperature. For rain clouds, a three dimensional interpolation is performed (i.e., including the effective radius dimension) for both extinction coefficient and single scattering albedo, but interpolation for the phase function (Legendre terms) is only performed if number of elements for the phase function (`n_Phase_Elements`) is greater than zero and the scattering flag (`Include_Scattering`) is set to `True`. The interpolation for Legendre terms is then performed as a function of temperature, frequency, and effective radius.

The current lookup tables for frozen hydrometeors include scattering parameters for snow, graupel and ice/hail (the same coefficients are used for ice and hail). Similar to `WATER_CLOUD`, the interpolation of extinction coefficient for `ICE_CLOUD` is performed using the lowest bin of effective radius in the lookup tables as a function of frequency. For the rest of the frozen hydrometeors, the interpolation is done as a function of both frequency and the effective diameter. Similar to rain clouds, the interpolation for Legendre terms is only performed if the number of phase elements is greater than zero and the scattering flag is set to `True`. The interpolation for Legendre terms is then performed as a function of frequency and effective radius.

The new DDA lookup tables include the backscattering coefficients in addition to the parameters included in the current lookup tables. Additionally, in the DDA lookup tables, instead of effective radius, the parameters are given as a function of the cloud water content in the unit of kg m^{-3}. The current Mie lookup tables include 5, 10, and 31 elements for temperature, effective radius, and frequency, respectively. The new DDA lookup tables are generated at much higher resolution with 8, 100, and 200 elements for temperature, water content and frequency, respectively.

3.2. The ARTS Database

The ARTS DDA database was developed by Eriksson et al. (2018) and includes single scattering properties for both frozen and liquid hydrometeors. The ARTS database covers a wide range of frequencies (1–866 GHz), temperatures (190 K, 230 K, and 270 K), and sizes. The frequencies were generally selected to match current and proposed passive MW and radar instruments. The database is developed for both passive and active MW instruments and provides scattering information for the full Stokes vector. The first version of the database is generated for 34 randomly oriented shapes but we selected 19 of the most common habits to include in CRTM, see Figure 1 for the list of selected habits. The liquid droplets are currently only represented by a spherical shape in the publicly available ARTS dataset (Ekelund, Brath, et al., 2020), but including non-spherical raindrops and melting particles is planned for the future releases (Ekelund, Eriksson, & Kahnert, 2020; Eriksson et al., 2018).

The ARTS database was generated using the package developed by Yurkin and Hoekstra (2011), known as the Amsterdam DDA (ADDA). The dataset includes about 35–45 different sizes for single crystal data and 35 sizes for the aggregates. The maximum diameter (D) can reach up to 10 mm for single crystal habits and 20 mm for aggregates but it depends on the frequency, see Eriksson et al. (2018) for details. The ARTS database includes the extinction matrix, the absorption vector, and the phase matrix as well as information on the temperature and frequency. It should be noted that some RT solvers may require the scattering parameters in a different format such as the single scattering albedo and the asymmetry parameter, but as discussed in Section 5, these parameters can be derived from what has been provided in the ARTS database. The ARTS dataset has also been implemented

Figure 1. Single crystal, aggregates, and liquid habits from the ARTS database included in the CRTM cloud lookup tables. The images for the individual habits were taken from the ARTS database (Eriksson et al., 2018).

in RTTOV (Radiative Transfer for TOVS) and it has been evaluated in the ECMWF data assimilation system (Geer, 2021; Geer et al., 2021). We limited the rain droplet size to 10 mm while calculating the bulk scattering properties because larger drop sizes may not be realistic. However, we used all the sizes provided in the database for all other habits.

3.3. The Liu Database

Liu (2008) generated the DDA optical properties database using the DDSCAT package (Draine & Flatau, 2000) for the frequency range of 15–340 GHz, five temperatures between 233 and 273 K, as well as 11 different particle shapes. The shaped used in Liu (2008) can be classified into "columns and plates", "rosettes", and "snowflakes". Liu (2008) considered two types of snowflakes including a sector-like particle and a dendrite snowflake. The sector-like snowflake was represented by three identical ellipsoids. The readers are referred to Figure 1 in Liu (2008) for the visual representation of the habits. As MW frequencies are almost insensitive to small particles, the database was generated for rather large ice particles so that the maximum diameter reaches up to 4,835 μm for the columns, 5,059 μm for the plates, 10,000 μm for the rosettes, and 12,454 μm for the dendrite snowflake. Since the Liu08 database only provides a limited number of habits that can be mostly considered as cloud ice, it cannot be used as a stand alone dataset to generate the scattering lookup tables required by CRTM. Therefore, we have only compared some individual Liu08 habits with their corresponding ones in the ARTS lookup tables.

3.4. Accuracy of the DDA Datasets

There are two possible causes for inaccuracy in the DDA calculations: (a) the interdipole spacing not being small enough and (b) lack of enough number of orientations to represent random orientations (Liu, 2008). Draine and Flatau (1994) recommend the following criteria to minimize the error due to the interdipole spacing: $|m|ks < 0.5$, where m is the refractive index, k is the wavenumber calculated as $2\pi/\lambda$ (λ is wavelength), and s is the dipole size which represents the interdipole spacing as well. This recommendation for the interdipole spacing has been followed by both Liu (2008) and Eriksson et al. (2018). Liu (2008) also reports that the effect of reducing the dipole size by half is less than 2% on scattering and absorption cross sections as well as asymmetry parameters when averaged over all frequencies and particle sizes. The orientation in DDSCAT is represented by three Euler angles and Liu (2008) performed 16, 17, and 16 orientations for different Euler angles. Liu (2008) concludes that doubling the number of orientations has an effect less than one percent on the results of absorption and scattering cross sections as well as asymmetry parameters. The ADDA package used by Eriksson et al. (2018) handles either fixed or random orientations. The random orientation starts with two scattering calculations for two angles in opposite directions (i.e., 180° apart), then the integrated average is iteratively updated adding new angles for scattering calculations until a convergence is achieved (Eriksson et al., 2018).

4. Radiative Transfer Equation

CRTM uses lookup tables for calculating atmospheric transmittance as well as scattering and absorption by clouds. These quantities are first calculated for individual layers based on the inputs provided to the model, then the RT solvers are used to integrate absorption and scattering by atmosphere and clouds from surface to the top of atmosphere. The Radiative Transfer Equation for a one dimensional atmosphere can be expressed in its derivative form as:

$$\mu \frac{\mathrm{d}I_v}{\mathrm{d}\tau} = -I_v(\tau,\Omega) + \frac{\omega}{4\pi}\int_0^{2\pi}\int_{-1}^{1} P\left(\tau;\Omega;\Omega'\right) I\left(\tau,\Omega'\right)\mathrm{d}\Omega' + S(\tau;\Omega;\Omega_0) \quad (1)$$

where, I is the intensity, τ is the optical thickness, μ is the cosine of the zenith angle θ, μ_0 is the cosine of the solar zenith angle, Ω is the beam solid angle accounting for both zenith (θ) and azimuth (ϕ), Ω_0 is the solar angle, ω is the single scattering albedo, P is the phase function, and S is the source function (Chandrasekhar, 2011; Liou, 2002; Liu et al., 2018). The source function in its general form, which includes the solar contribution as well, can be expressed as:

$$\mathbf{S} = (1-\bar{\omega})\, B(T_\tau) + \frac{\bar{\omega} F_0}{4\pi} e^{-\tau/\mu_0} P(\Omega,\Omega_0) \quad (2)$$

where, T_τ is the temperature at layer τ, B is Planck function, and F_0 is solar spectral constant (Liu et al., 2018). There is no analytical solution for Equation 1, thus this equation can only be solved using numerical methods also known as scattering solvers (Heidinger et al., 2006; Liu & Weng, 2006; Stamnes et al., 1988).

CRTM includes two scattering solvers, the Advanced Doubling Adding (ADA) Method (Liu & Weng, 2006) and the Successive-Order-of-Interaction (Heidinger et al., 2006). The default scattering solver in CRTM is currently the ADA method which requires extinction coefficient, single-scattering albedo, and phase function in terms of Legendre polynomials to perform scattering calculations. The current version of the CRTM neither considers three dimensional scattering due to inhomogeneity in clouds and surface, nor the polarization induced due to clouds and other particles.

5. Bulk Optical Properties

The mathematical description of the DDA technique is beyond the scope of this paper, but in its simplest form the extinction (σ_e) and absorption (σ_a) cross sections are calculated within the DDA technique as follows (Yurkin & Hoekstra, 2011):

$$\sigma_e = 4\pi k \Sigma_i \left(P_i E_i^{inc*} \right) \tag{3}$$

$$\sigma_a = 4\pi k \Sigma_i \left(P_i E_i^{*} \right) \tag{4}$$

where, E^{inc} and E are the incident and total electric field, $*$ denotes complex conjugate, P is the polarization of the subvolume i, and k is the free-space wave vector (Penttilä et al., 2007; Yurkin & Hoekstra, 2007). The ADDA package provides absorption and extinction cross sections as well as Mueller matrix (**M**) and amplitude scattering matrix (**S**). The scattering cross section (σ_s) can be calculated either as $\sigma_s = \sigma_e - \sigma_a$ or using the Mueller matrix as follows:

$$\sigma_s = \frac{1}{\kappa^2} \int_{4\pi} M_{11} dn' \tag{5}$$

where κ is the wavenumber. Likewise, the phase matrix (**Z**) is calculated using the Mueller matrix as follows:

$$\mathbf{Z} = \frac{1}{\kappa^2} \mathbf{M} \tag{6}$$

Now, the backward and forward scattering cross sections, σ_{bs} and σ_{fs}, respectively, are simply equal to the first element of the phase matrix (Z_{11}) at specific scattering angles (θ) of 180° and 0.0°:

$$\sigma_{bs} = Z_{11}(\theta = 180) \tag{7}$$

$$\sigma_{fs} = Z_{11}(\theta = 0.0) \tag{8}$$

The single scattering efficiencies (Q) as well as the size parameter (x) are then calculated as:

$$Q = \frac{4\sigma}{\pi D_{veq}^2} \tag{9}$$

$$x = \frac{\pi D_{veq}}{\lambda} \tag{10}$$

$$D_{veq} = \left(\frac{6m}{\pi \rho} \right)^{1/3} \tag{11}$$

where σ is the cross section (in m^2) for absorption, extinction, or scattering, m is the mass of particles (in kg), λ is wavelength (in m), ρ is the density that varies with particle size, and D_{veq} is volume equivalent diameter (in m). These relations ensure that both x and Q are calculated with respect to D_{veq} and are unitless. The single scattering efficiencies are not directly used to calculate the bulk scattering properties, but are used in Section 6.1 to discuss the optical properties of the ARTS database.

The bulk extinction β_e, scattering β_s, and absorption β_a coefficients are then calculated by integrating over the number density of particles per unit diameter of particle (m^{-3} m^{-1}), $n(D)$:

$$\beta_y = \int_0^\infty \sigma_y(D)n(D)dD \tag{12}$$

where D represents the maximum diameter defined as the diameter of smallest sphere that can enclose the particle and subscript y refers to extinction, absorption, and scattering. Note that although the particles are theoretically integrated from 0 to ∞, in practice the scattering database includes a limited number of sizes so the integration is performed from $D_{\min}$ to $D_{\max}$. The number density $n(D)$ is estimated using the particle size distributions (PSDs) which are discussed in Section 5.1.

CRTM requires mass scattering coefficients which can be calculated by dividing bulk extinction, absorption, and scattering coefficients by water content (Ψ, also see Equation 32) which itself can be calculated as follows:

$$\Psi = \int m(D)n(D)dD \tag{13}$$

where the mass of individual particles can be calculated as $m(D) = \alpha D^\beta$ (coefficients α and β describes the mass-size relation and are provided in the DDA database for each habit). The mass scattering coefficients (k_y in m^2 kg^{-1}) then can be calculated as follows:

$$k_y = \frac{\beta_y}{\Psi} = \frac{\int \sigma(D)n(D)d\,D}{\int m(D)n(D)d\,D} = \frac{\int \sigma(D)n(D)d\,D}{\int \rho(D)V(D)n(D)d\,D} \tag{14}$$

where the volume V can be calculated as $V = \pi D^3/6$ and density ρ varies with the particle size such that $\rho = m(D)/V(D)$. Other parameters required by CRTM include asymmetry factor (g) and single scattering albedo (ω). The bulk asymmetry factor or parameter (g_{bulk}) is calculated using the single asymmetry factor (g) and PSD as follows:

$$g = \frac{1}{4\pi}\int_0^{2\pi}\int_{-\pi/2}^{\pi/2} P\cos\theta\sin\theta d\theta d\phi \tag{15}$$

$$g_{bulk} = \frac{\int g(D)\sigma_s(D)n(D)dD}{\int \sigma_s(D)n(D)dD} \tag{16}$$

where θ and ϕ are the zenith and azimuth angles and P is the normalized phase function.

Single scattering albedo (ω) is the ratio of scattering to extinction cross section ($\omega = \sigma_s/\sigma_e$) and the bulk ratio ($\omega_{bulk}$) can be calculated as:

$$\omega_{bulk} = \frac{k_e - k_a}{k_e} = \frac{k_s}{k_e} = \frac{\int \omega(D)\sigma_e(D)n(D)dD}{\int \sigma_e(D)n(D)dD} \tag{17}$$

CRTM also requires phase function represented using Legendre Polynomials. Since CRTM calculations are performed for unpolarized radiances, only the first element of the phase matrix (Z_{11}) is required. This is in turn weighted as follows:

$$P_{11} = \frac{4\pi Z_{11}}{\sigma_s} \tag{18}$$

The bulk phase function ($P_{11,bulk}$) then can be calculated as:

$$P_{11,bulk} = \frac{\int P_{11}(D)\sigma_s(D)n(D)dD}{\int \sigma_s(D)n(D)dD} \tag{19}$$

Since CRTM prescribes the phase function in terms of Legendre polynomials, the bulk Legendre terms (L_{bulk}) can be directly calculated as follows:

$$L_{j,bulk} = \frac{\int L_j(D)\sigma_s(D)n(D)dD}{\int \sigma_s(D)n(D)dD} \tag{20}$$

where L_j is the jth Legendre polynomial for a single particle with the maximum dimension D. Note that even the first element of the phase function is a vector depending on the scattering angle, therefore Equations 18–20 need to be repeated for different scattering angles.

5.1. Particle Size Distributions

PSDs are used to calculate the number density of particles per unit diameter of the particles, $n(D)$ with the unit $m^{-3}\ m^{-1}$ or m^{-4} for simplicity, which is necessary to calculate the bulk scattering properties required by CRTM. We used the mid-latitude version of Field et al. (2007) to compute the PSD for the frozen particles and Abel and Boutle (2012) to calculate the drop size distribution for rain.

Field et al. (2007) developed a two moments PSD using the aircraft measurements from mid-latitude and tropical campaigns for frozen hydrometeors. The Field et al. (2007) PSDs require second and third moments (M_2 and M_3, respectively). The βth moment is computed using cloud water content as $IWC = \alpha M_\beta$ (α and β are the mass-size relation coefficients). M_2 is equal to M_β if $\beta = 2$, otherwise the following relation will be used to calculate both M_2 and M_3 from M_β:

$$M_n = A(n)\exp\left(B(n)T_c\right) M_2^{C(n)} \tag{21}$$

$$A(n) = \exp\left(13.6 - 7.76n + 0.479n^2\right) \tag{22}$$

$$B(n) = -0.0361 + 0.0151n + 0.001n^2 \tag{23}$$

$$C(n) = 0.807 + 0.00581n + 0.0457n^2 \tag{24}$$

where, T_c is temperature in °C, M_n is the moment of n to be predicted, and all the constants (A, B, and C) only depends on n. The particle density then can be calculated using the second and third moments as well as the dimensionless size (x) and the rescaled dimensionless concentration (Φ) as follows:

$$n(D) = \Phi_{23}(x)\frac{M_2^4}{M_3^3} \tag{25}$$

$$x = D\frac{M_2}{M_3} \tag{26}$$

$$\Phi_{23}(x) = 152\exp(-12.4x) + 3.28x^{-0.78}\exp(-1.94x) \quad \text{Tropical} \tag{27}$$

$$\Phi_{23}(x) = 141\exp(-16.8x) + 102x^{-2.07}\exp(-4.82x) \quad \text{Midlatitude} \tag{28}$$

We used Abel and Boutle (2012) gamma distribution for the raindrop size distribution (DSD) which can be expressed as:

$$n(D) = N_0 D^\mu \exp(-\lambda D) \tag{29}$$

where n(D) indicates the number concentration of raindrops as a function of diameter, N_0 is the intercept, λ is the slope, and μ is the shape parameter of the distribution. The intercept (N_0) is then calculated from the mass mixing ratio of rain (q_R):

$$N_0 = \left(\frac{N_1 - N_2}{2}\right)\tanh\left[\frac{q_{R0} - q_R}{4q_{R0}}\right] + \frac{N_1 + N_2}{2} \tag{30}$$

As recommended by Abel and Boutle (2012), N_1, N_2, and q_{R0} are set to 9×10^9 m^{-3} m^{-1}, 2×10^6 m^{-3} m^{-1}, and 1×10^{-4} kg kg^{-1}, respectively. The slope parameter (λ) is then calculated using the following relation by assuming $x_1 = N_0$, $x_2 = 0$, and $\mu = 0$:

$$\lambda = \left[\frac{\pi \rho_w x_1 \Gamma(4+\mu)}{6 \rho_{air} q_R}\right]^{\frac{1}{4+\mu-x_2}} \tag{31}$$

where, Γ is the Gamma function, and ρ_{air} and ρ_w are the densities of air (1.225 kg m^{-3} and liquid water (1,000 kg m^{-3}).

Geer et al. (2021) suggest using the ratio of input water content (Ψ) to implied or computed water content (Ψ_c), $r = \Psi/\Psi_c$, to scale the calculated n(D) as $n'(D) = n(D) \times r$. The implied water content (Ψ_c) can be calculated using the mass of the particles and number density as follows:

$$\Psi_c = \int_{D_{\min}}^{D_{\max}} m(D) n(D) dD = \int_{D_{\min}}^{D_{\max}} \alpha D^{\beta} n(D) dD \tag{32}$$

The mass of particles, $m(D)$, may not necessary be equal to αD^{β} if the mass is provided by the DDA recorded mass.

The maximum values for the order of magnitude of renormalization $|log10(r)|$ for different habits are shown in Table 1. Most habits show a renormalization magnitude less than 0.1, except for `SectorSnowflake`, `LargePlateAggregate`, `LargeBlockAggregate`, and `LargeColumnAggregate` with a magnitude of renormalization greater than 0.3. The maximum renormalization orders found by Geer et al. (2021) were also mostly less than 0.1 but there were orders reaching nearly 0.5 for the Field et al. (2007) tropical PSD and up to 9.1 for the Field et al. (2005) PSD. Hence these results seem consistent and the explanation for different renormalization factors is unlikely to be the approach to numerical integration, but rather the choice of PSD.

In addition to mid-latitude version of Field et al. (2007) and Abel and Boutle (2012), several other PSDs were examined including Field et al. (2007). Tropical, Field et al. (2019), McFarquhar and Heymsfield (1997), and modified gamma distribution recommended by Geer et al. (2021). In most cases, the water content calculated using the number density (Equation 32) was a few order of magnitude different from the water content used as input to estimate the PSD parameters. Field et al. (2007) which was parameterized using measurements from the tropical campaigns generally performed satisfactory for most habits, excluding some snow types such as GemSnow. GemSnow has a much larger forward scattering especially for small particles and its phase function has a very strong peak where the scattering angle is close to zero degrees. The mid-latitude version of Field et al. (2007) generally better distributes the mass between smaller and larger particles than the tropical version, helping to smooth out the peak of the phase function. This helps the Legendre polynomials with limited number of degrees (16°) to better fit the phase function. Otherwise, a relatively large difference (up to 30%) was introduced between the phase function reconstructed from the Legendre polynomials and the original phase function.

6. Results

The ARTS database provides the scattering parameters with different resolutions for frequency and size dimensions, however CRTM requires these parameters to be provided for all the habits in consistent grids for frequency, temperature (liquid clouds), and effective radius or water content. Therefore, the first step in generating CRTM cloud coefficients from the DDA database was to properly interpolate the scattering parameters to common grids of frequency and temperature. Current CRTM cloud coefficients use the effective radius for the interpolation of scattering properties over the mass/size dimension. However, the effective radius is not often provided by the NWP models as output, therefore different relations have been developed to estimate effective radius from parameters such as temperature and water content (Kim et al., 2020; Sieron et al., 2017). In addition, using model prognostic variables such as cloud water content (instead of effective radius) in the scattering lookup tables has been a standard practice in other fast radiative transfer models such as RTTOV for several decades (Bauer et al., 2006). Therefore, we modified CRTM to use cloud water density, referred to as cloud water content as well and defined as mass per volume (kg m^{-3}), for the mass dimension of the cloud lookup tables. The mass scattering parameters of the CRTM DDA lookup tables are then interpolated based on the cloud water content profiles provided as input

Table 1
List of the ARTS Habits Implemented Into the New CRTM Cloud Coefficient

Id	CRTM cloud name	ARTS habit name	Renorm	D_{min}	D_{max}
PT1	PlateType1	PlateType1	0.02409	13.2	10,000.0
CT1	ColumnType1	ColumnType1	0.00963	14.4	10,000.0
SBR	SixBulletRosette	6BulletRosette	0.02391	15.6	10,000.0
P4BR	Perpendicular4_BulletRosette	Perpendicular4BulletRosette	0.02555	18.0	10,000.0
F3BR	Flat3_BulletRosette	Flat3BulletRosette	0.02674	19.9	10,000.0
ICI	IconCloudIce	IconCloudIce	0.02311	12.9	10,000.0
SS	SectorSnowflake	SectorSnowflake	0.26293	20.0	10,238.0
ESA	EvansSnowAggregate	EvansSnowAggregate	0.02616	32.0	11,755.3
ECA	EightColumnAggregate	8ColumnAggregate	0.00165	19.4	9714.3
LPA	LargePlateAggregate	LargePlateAggregate	1.17367	349.1	22,859.7
LCA	LargeColumnAggregate	LargeColumnAggregate	0.70131	368.4	19,980.7
LBA	LargeBlockAggregate	LargeBlockAggregate	1.44166	348.6	21,875.9
ISN	IconSnow	IconSnow	0.17836	120.0	19,999.7
IH	IconHail	IconHail	0.09865	120.0	5349.1
GG	GemGraupel	GemGraupel	0.07473	120.0	6596.7
GS	GemSnow	GemSnow	0.12869	169.7	10,458.6
GH	GemHail	GemHail	0.1083	120.0	5031.4
IS	IceSphere	IceSphere	0.00075	1.0	47,354.0
LS	LiquidSphere	LiquidSphere	0.00063	1.0	47,354.0
SC	SNOW_CLOUD	LargePlateAggregate	1.17367	349.1	22,859.7
GC	GRAUPEL_CLOUD	GemGraupel	0.07473	120.0	6596.7
HC	HAIL_CLOUD	GemHail	0.1083	120.0	5031.4
IC	ICE_CLOUD	IceSphere	0.00075	1.0	47,354.0
WC	WATER_CLOUD	LiquidSphere	0.00063	1.0	47,354.0
RC	RAIN_CLOUD	LiquidSphere	0.00063	1.0	47,354.0

Note. The defaults for the CRTM common cloud types are also included in the end of the table. The maximum values for the order of magnitude of renormalization (*Renorm*) were calculated based on the Field et al. (2007) mid-latitude PSD for frozen hydrometeors and the Abel and Boutle (2012) PSD for liquid hydrometeors.

to CRTM. Layer-integrated cloud water content (kg m^{-2}) is already required as input to CRTM for performing the scattering calculations and cloud water density can be calculated as the layer-integrated cloud water content divided by the layer thickness. Therefore, using cloud water density for the mass dimension of the lookup tables does not demand any new input parameter for the CRTM all-sky simulations.

Table 1 includes the list of cloud types that can be defined in CRTM control files when the ARTS scattering lookup tables are used. This table also indicates the corresponding ARTS habits for the CRTM default clouds, that is, `SNOW_CLOUD`, `GRAUPEL_CLOUD`, `HAIL_CLOUD`, and `ICE_CLOUD`. The new cloud coefficient covers a frequency range of 1.0–200 GHz with a resolution of 1.0 GHz. The water content ranges from 10^{-6} kg m^{-3} to 10^{-2} kg m^{-3} with 200 elements equally spaced in the logarithmic scale. The optical properties of the liquid clouds were generated for temperatures of 230, 240, 250, 260, 270, 280, 290, and 300 K. We used a Piecewise Cubic Hermite Interpolating Polynomial (Fritsch & Butland, 1984) for interpolation over the frequency and size dimensions and linear spline for interpolating over the temperature dimension. These two interpolation techniques do not produce artifacts when generating high resolution grids of frequency and temperatures. The only exception is for the PlateType1 with some artifacts observed for the low frequencies. CRTM does not take into account the temperature dependency of the optical properties of frozen hydrometeors, therefore we chose 260 K as the reference temperature to generate the scattering lookup tables for frozen hydrometeors.

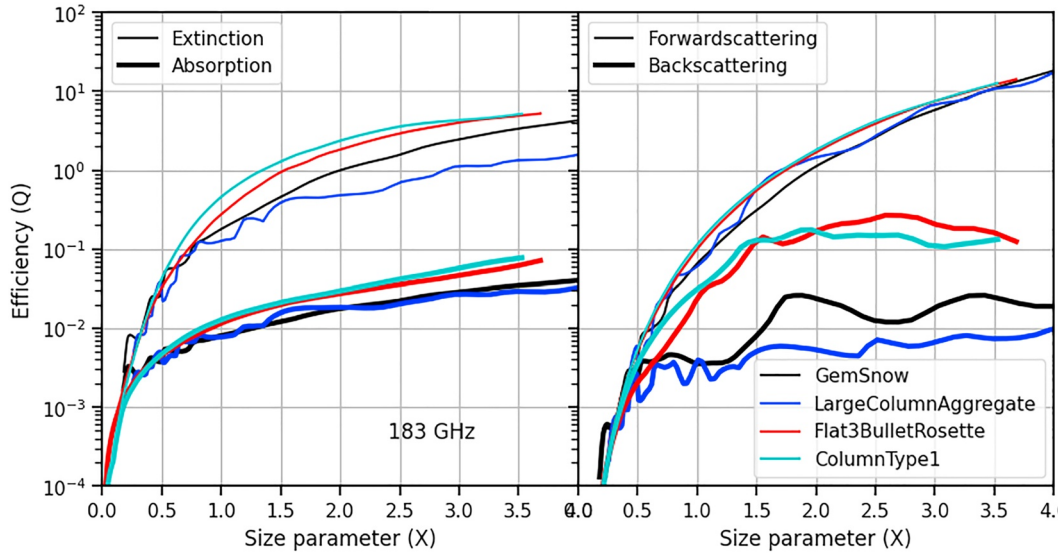

Figure 2. Extinction, absorption, forwardscattering, and backscattering efficiencies for different ARTS habits computed at a frequency of 183 GHz and a temperature of 260 K. Both size parameter (X) and single scattering efficiencies (Q) are unitless.

6.1. ARTS Single Scattering Properties

The extinction, absorption, forward-scattering, and backscattering efficiencies calculated using the ARTS database for a few different ARTS habits are shown in Figure 2 and the same parameters for the rest of the ARTS habits are shown in Figure A1 in Appendix A. The scattering parameters shown in these figures were computed for a temperature of 260 K and a frequency of 183 GHz. Overall, all four scattering parameters rapidly change with the size parameter so that they are almost negligible for small size parameters (less than 0.5). This will translate to insensitivity of MW spectrum to small particles if accompanied with low number density. However, in practice the number of smaller particles can be orders of magnitude higher which will compensate for this, for example, see Figure 2 in Ekelund, Eriksson, and Pfreundschuh (2020). GemSnow and LargeColumnAggregate show lower absorption and extinction than Flat3BulletRosette and ColumnType1. The liquid clouds generally show much higher absorption than frozen clouds (see Figure A1). The forward and backward scatterings are calculated for phase function at 0.0° and 180°, respectively. The forward scattering is generally dominant, especially for GemSnow and LargeColumnAggregate with relatively lower backscattering than Flat3BulletRosette and ColumnType1. A combination of forward and backward scattering can be used to determine which habits cause larger or smaller scattering. While backward scattering removes the scattered signal from the direction of propagation, the MW signal scattered forward will be still within the field of view of the instrument (the same direction of propagation).

6.2. CRTM Bulk Scattering Properties

The mass scattering parameters for several ARTS habits, parameters actually stored into CRTM cloud coefficients, are shown in Figure 3. In addition to these parameters, Legendre coefficients for the phase function are also stored in the cloud coefficient files. These parameters for the rest of the ARTS habits are shown in Figure A2 in Appendix A. Figure 3 includes the mass scattering parameters for two different frequencies, 183 and 90 GHz, and the difference among scattering parameters for different frequencies clearly shows the frequency dependency of these parameters. The liquid clouds (rain clouds) generally have much higher absorption values than frozen clouds. The mass extinction and absorption coefficients for liquid clouds are also very close, especially for low cloud water content values, showing little scattering for small rain/liquid particles. The extinction and absorption coefficients for frozen clouds are clearly much larger at 183 GHz than at 90 GHz. The single scattering albedo values are very small for liquid sphere confirming little scattering for these type of clouds. The habits presented in Figure 3 (especially GemSnow and CloudType1) indicate a single scattering albedo close to unity at 183 GHz for cloud water content values greater than 10^{-4} kg m^{-3}. This shows large scattering to extinction ratio

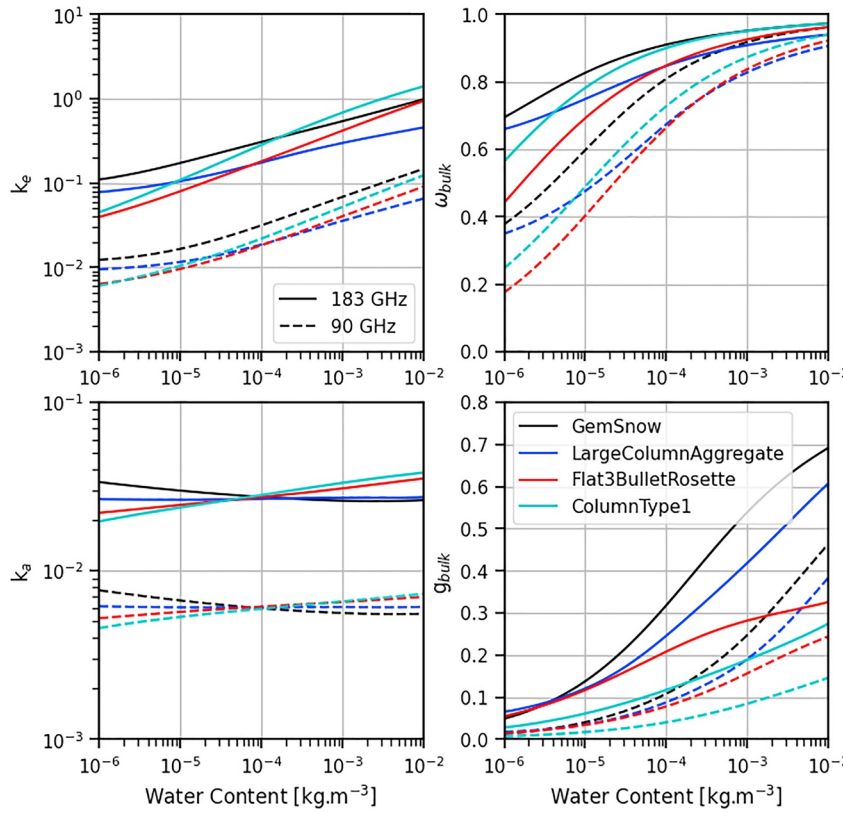

Figure 3. The mass extinction and absorption coefficients (both in $m^2\ kg^{-1}$) as well as bulk single scattering albedo and asymmetry factor (both unitless) for several habits at 260 K.

for these habits at high frequencies like 183 GHz. Again, the larger scattering coefficients only translates to larger scattering signal if the forward scattering is not dominant compared with backward scattering.

Figure 4 shows the bulk phase function for two different habits as well as several frequencies versus scattering angle. It also shows the differences between the phase functions constructed using the Legendre polynomials with 16° and the original bulk phase functions used to compute the Legendre coefficients. GemSnow shows a much stronger forward scattering than GemHail for higher frequencies (180 GHz), however the differences are smaller for the lower frequency channels. The difference between Legendre fit and original phase function is less than 0.2% with the differences being larger for higher frequencies than the lower frequencies. The reason for spikes in the errors is that Legendre fits wiggle around the original phase functions so that the error fluctuates between zero and its maximum. The magnitude of error would significantly decrease if we increase the degree of Legendre polynomials, but this would require a substantial code change in CRTM and the small fitting errors for Legendre polynomials do not justify this effort. However, a polarized version of CRTM is under development that may require re-evaluating the degree of Legendre polynomials.

6.3. Sensitivity of MW Observations to Clouds

The sensitivity of MW observations to clouds varies as a function of shape/habit, size, and orientation of the particles as well as the frequency of channels. In order to evaluate the sensitivity of MW radiances to clouds over the rainbands of tropical cyclones, we used the IFS simulations over the rainbands of Hurricane Irma on 7 September 2017 at 18:00 UTC. We conducted a series of CRTM simulations by assigning different IFS cloud water content values to their corresponding habits in the ARTS DDA database. This included assigning the rain water content (both convective and large scale) to `RAIN_CLOUD`, cloud liquid water content to `LIQUID_CLOUD`, cloud ice water content to either `ICE_CLOUD` or `IceSphere`, large scale snow water content to different habits suitable for falling snow, and splitting the convective snow water content between `HAIL_CLOUD` and `GRAUPEL_CLOUD`. The ARTS equivalent for the default CRTM cloud types are shown in Table 1. These simulations

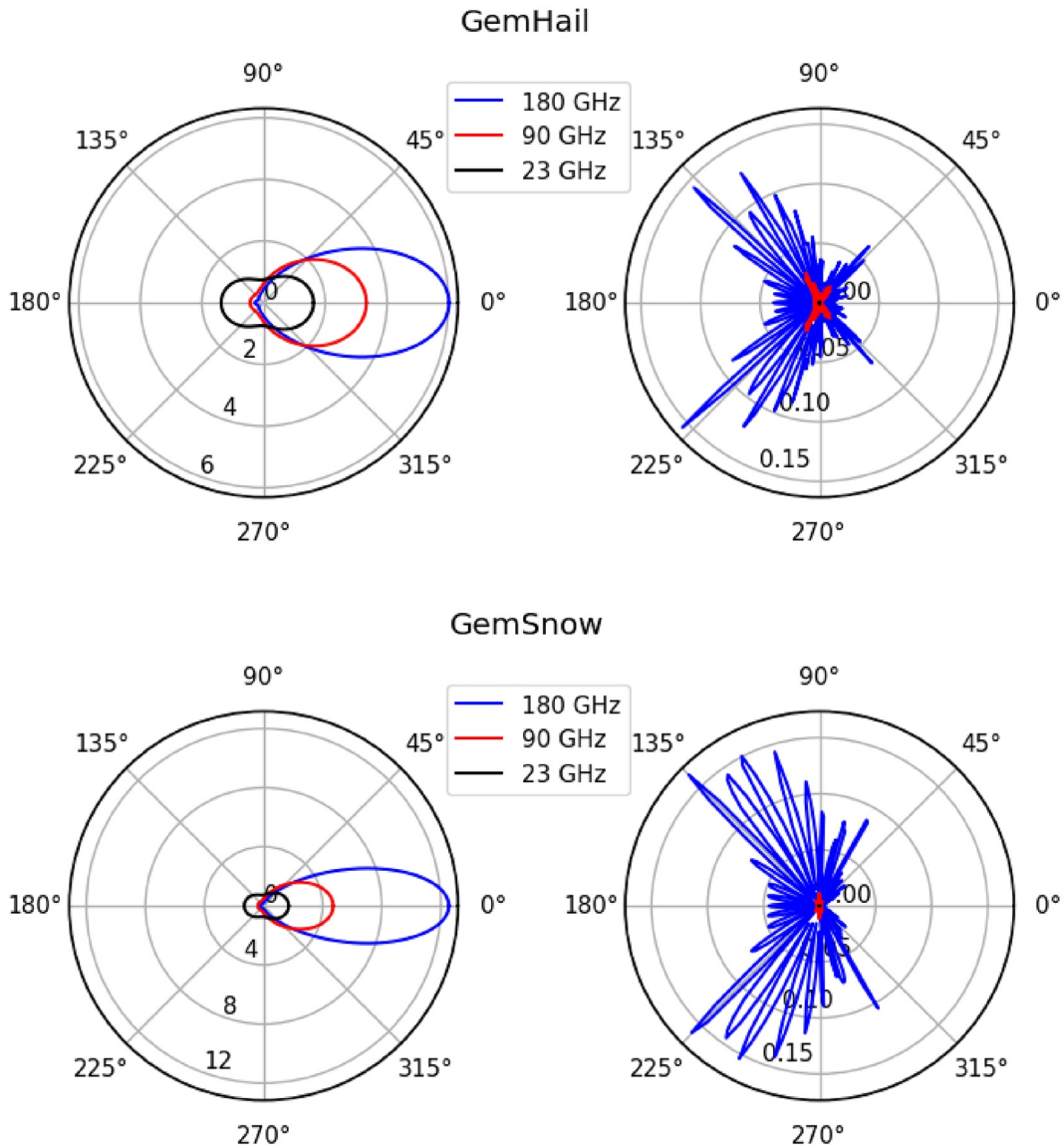

Figure 4. Bulk phase function (left) and the error of the phase functions reconstructed using the corresponding Legendre polynomials (right) for GemHail (top) and GemSnow (bottom). The error was calculated as the differences between the original phase function minus the one constructed using the Legendre polynomials. Different colors indicates different frequencies. The values plotted are for a cloud water content of 5×10^{-3} kg m^{-3}.

were once conducted for the ATMS instrument and once for a hypothetical instrument with a large number of channels and a spectral coverage of 10–250 GHz.

Figure 5 shows the results for the hyperspectral instrument after being averaged over the entire domain (rainbands) of Hurricane Irma and presented as a function of channels' frequency. The all-sky simulations (`ALL-SKY`) in Figure 5 were conducted using an ensemble of clouds by assigning the IFS water content values to corresponding ARTS/CRTM habits as explained in the previous paragraph. In this case, the large-scale snow water content was assigned to `LargePlateAggregate`. All other simulations were performed using a single hydrometeor type. For instance, only large scale snow water contents were used to run the simulations for `SectorSnowflake` using the sector snowflake habit and all other hydrometeors (hail, graupel, ice, rain, liquid) were excluded from the scattering calculations. Similarly, `MIE:SNOW_CLOUD` indicates the simulations using Mie lookup tables with large-scale snow water content being assigned to `SNOW_CLOUD`. In case of clear sky simulations, all clouds were excluded in the calculations by setting number of clouds in CRTM to zero. The top panel in Figure 5 shows

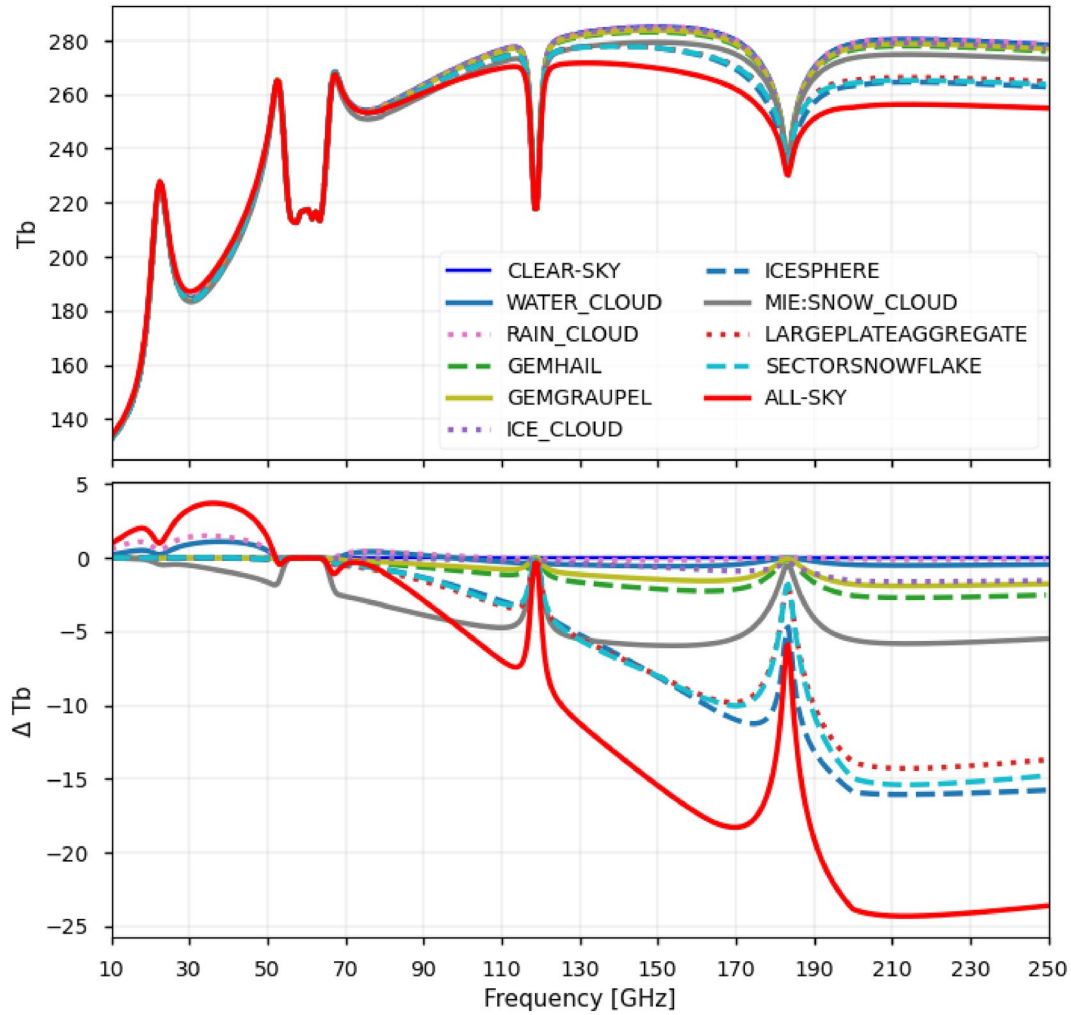

Figure 5. The cloud signal as a function of frequency calculated using the ARTS DDA database for different habits. The top panel shows the actual brightness temperatures (Tb) simulated for specific habits/shapes and the lower panel shows the cloud signal (ΔTb). The cloud signal is calculated as the cloudy simulations conducted using a single habit/shape minus clear-sky brightness temperatures. The all-sky simulations (`ALL-SKY`) shows the simulations conducted using an ensemble of clouds and `MIE:SNOW_CLOUD` shows the simulations using the Mie lookup tables for `SNOW_CLOUD`.

the actual brightness temperatures and the lower panel shows the cloud signal calculated as cloud contaminated brightness temperatures minus clear-sky brightness temperatures. In this figure, both `ICE_CLOUD` and `IceSphere` utilize the scattering properties of `IceSphere` but CRTM only considers the lowest bin in lookup tables for `ICE_CLOUD`. The cloud type shown as `MIE:SNOW_CLOUD` uses the Mie lookup tables but all other simulations were performed using the ARTS DDA lookup tables.

The measured or simulated brightness temperatures in the MW spectrum in clear-sky are affected by surface emissivity, water vapor continuum, and a few distinct absorption bands including water vapor absorption bands at 22 and 183 GHz, and oxygen absorption bands around 60 and 118 GHz. It should be noted that Figure 5 is generated using a subset of very moist atmospheric profiles over the oceanic rainbands of Irma. The shape of the spectrum can significantly vary if this figure is generated using simulations from dry atmospheric profiles or profiles over land. Nevertheless in this specific case, water vapor absorption at 22 GHz helps to lift the weighting functions from the radiometrically cold surface of the ocean with a very low emissivity, therefore causes the brightness temperatures for channels operating close to the water vapor absorption band at 23 GHz to be warmer than the brightness temperatures for adjacent frequencies. Both oxygen bands and water vapor absorption band at 183 GHz overall lower the brightness temperatures for corresponding channels. The weighting function for the channels operating near the center of the oxygen bands peak high in the atmosphere so that these channels are

either insensitive to clouds or are not as sensitive to clouds as channels with the weighting functions peaking in the mid or lower troposphere.

Figure 6 shows the spatial distribution of the differences between cloudy and clear-sky simulations performed using the ARTS lookup tables (the same simulations used in Figure 5 but not spatially averaged). The first row shows the difference between all-sky simulations and clear-sky simulations. The third to last rows show the differences between simulations performed using individual cloud types and clear-sky simulations. All the simulations were conducted using the ARTS lookup tables, except for `MIE-SC` that used `SNOW_CLOUD` from the Mie lookup tables and `LIU08-SS` that was conducted using the `SectorSnowflake` from the Liu08 lookup table. Note that the color-bars are in logarithmic scale, red color showing emissions (when cloudy brightness temperatures are higher than the clear-sky simulations) and blue color showing scattering (cloud contaminated brightness temperatures are colder than clear-sky simulations). The abbreviations used in Figure 6 are defined in Table 1.

Figures 5 and 6 show that the frequencies below 90 GHz are mostly affected by emission from `RAIN_CLOUD` and `WATER_CLOUD`, and frequencies above 90 GHz are mainly affected by scattering from frozen hydrometeors. Although, hail and graupel may, on average, only introduce a few kelvin difference in brightness temperatures (Figure 5) but that is because the mass mixing ratios for convective snow clouds that are used to define the water content profiles for hail and graupel (see Figure 6) are relatively low. The snow clouds (SectorSnowFlake and LargePlateAggregate) show a major depression in brightness temperatures both in Figures 5 and 6. Both `ICE_CLOUD` and `IceSphere` use the same water content profiles and `ICE_CLOUD` also uses the scattering properties from `IceSphere` in the ARTS lookup tables. The difference between the two is because of special treatment of CRTM for `ICE_CLOUD`. This clearly shows that taking the lowest bins from the lookup tables for `ICE_CLOUD` largely eliminates the scattering affect from the ice water content. Therefore, it is highly recommend to use `IceSphere` when running CRTM with the ARTS DDA lookup tables.

The Mie lookup tables show sensitivity to snow clouds (`MIE-SC`) all the way down to 10 GHz. In addition, unlike the DDA lookup tables for snow habits, the sensitivity to snow clouds does not substantially change above 130 GHz for the Mie lookup tables, except for the channels operating on the 183 GHz band, see Figure 5. Figure 6 also includes the `SectorSnowflake` from Liu08 database for the comparison between Liu08 and ARTS lookup tables. The scattering properties of `SectorSnowflake` from the Liu08 database (`LIU08-SS`) are almost identical to that of `SectorSnowflake` from ARTS. The same conclusion also applies to the `Flat-3BulleteRosette` showing that although ARTS and Liu08 databases were generated using two different DDA packages, the results are independent of what package was used to generate the DDA single scattering properties.

Rain introduces some noticeable emission for the lower frequency channels (especially channel 1 to 4) as well as some minor emission (over the rainbands) and scattering (near the core of the cyclone) for channel 16. Water clouds show a large emission signal in simulated brightness temperatures for channels 1–4 and to a lower extent channel 16. Water clouds also show some small scattering signals near the core of the cyclone. The scattering signal of all the clouds together (first row) show an emission signal for channels 1–4 and the outer rainbands of the cyclone for channel 16 and scattering signal for channels 16 and above. They also show a scattering signal for channels near the oxygen absorption band at 60 GHz, but the effect diminishes for the channels operating closer to the center of the band.

6.4. Effect of Temperature Dependency and PSD on Simulations

We generated the CRTM lookup tables for frozen habits using the fixed temperature of 260 K and Field 2007 PSD, which means that we do not model temperature dependencies of the optical properties or of the PSD. In order to explore the impact of PSD and also dropping any temperature dependence, we generated two new sets of lookup tables for frozen particles, one using a reference temperature of 240 K and Field et al. (2007) PSD (hereafter referred to as F240) and another set using the PSD used in the Geophysical Fluid Dynamics Laboratory (GFDL) cloud microphysics scheme (Zhou et al., 2022) and a reference temperature of 260 K (hereafter refereed to as G260). The original lookup tables were generated using a reference temperature of 260 K and Field et al. (2007) PSD (hereafter refereed to as F260). We then performed a new set of all-sky simulations similar to what was explained in Section 6.3 for a hyper-spectral MW instrument.

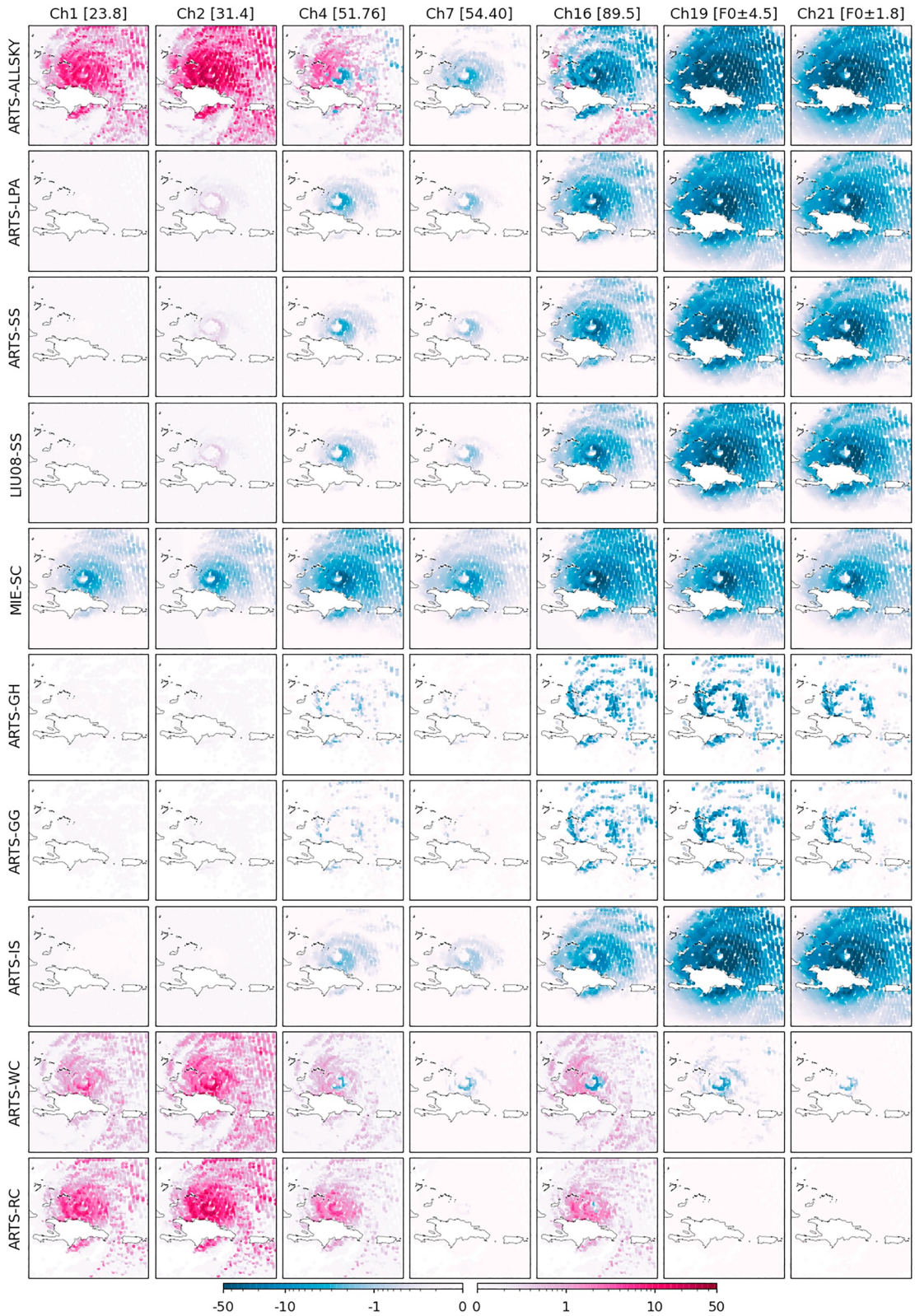

Figure 6.

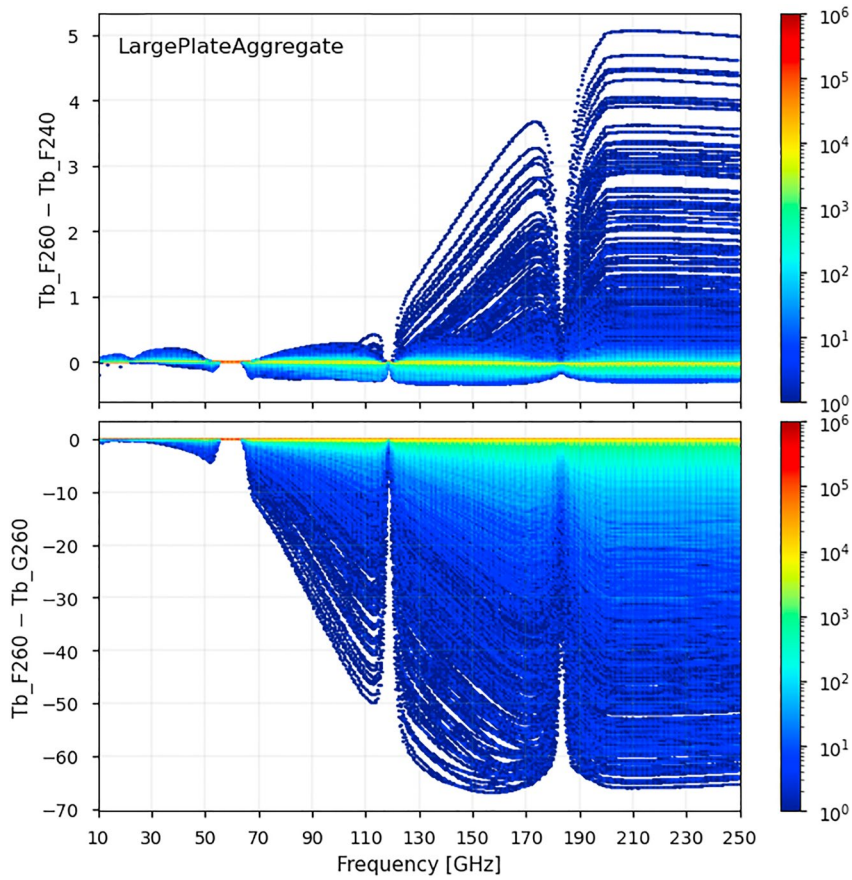

Figure 7. Difference in simulated brightness temperatures due to the choice of reference temperature or PSD used to generate the cloud lookup tables. The results are for all-sky simulations with LargePlateAggregate being used to prescribe the snow water content. Tb_F260 and Tb_F240 show the brightness temperatures simulated using lookup tables generated using Field et al. (2007) PSD and a reference temperature of 260 and 240 K, respectively, and Tb_G260 shows the brightness temperatures simulated using a reference temperature of 260 K and Zhou et al. (2022) PSD. The colorbars show number of occurrences as a function of channels' frequency.

The top panel in Figure 7 shows the difference between F260 and F240 as a function of frequency, which indicates the effect of temperature dependency of scattering properties of frozen particles on simulated brightness temperatures. We only used the profiles where sum of the snow and ice water contents was greater than zero. The differences are generally small, less than 0.5 K for most cases, but some of the profiles show a large difference up to 5 K for channels with a frequency above 120 GHz. The differences are also small for channels that are not too sensitive to the frozen hydrometeors, for instance channels near 183 and 118 GHz with weighting functions peaking largely above the clouds. The lower panel in Figure 7 shows the difference in simulated brightness temperatures due to the choice of PSD (F260-G260). The brightness temperatures simulated using F260 are overall lower than those simulated using G260. The differences are overall less than 10 K for most cases but there are profiles where the differences can reach up to 65 K. Again the sensitivity is lower for the channels close to 118 and 183 GHz where the weighting functions peak generally above the clouds.

The cases with differences larger than 0.5 K for temperature dependency and 30 K for the PSD dependency were identified to be the profiles located over the rainbands of Hurricane Irma with a mid tropospheric (500 hPa) temperature near the melting point (273 K). We selected 500 hPa temperature for analysis because most of the

Figure 6. Cloud signal estimated using the difference between simulated cloudy and clear-sky brightness temperatures. The first row from the top shows the difference between all-sky and clear-sky simulations and the other rows show the difference between simulations performed using individual clouds and clear-sky simulations. LIU08-SS and MIE-SC indicate the simulations conducted using the Liu08 SectorSnowflake and the Mie SNOW_CLOUD, respectively. All other simulations were performed using the ARTS lookup tables. The abbreviations for habits are included in Table 1. The ATMS channel numbers are printed on the top of each column and the frequency of each channel is given within the brackets in GHz (F0 is equal to 183.31 GHz). All the colorbars have a unit of Kelvin.

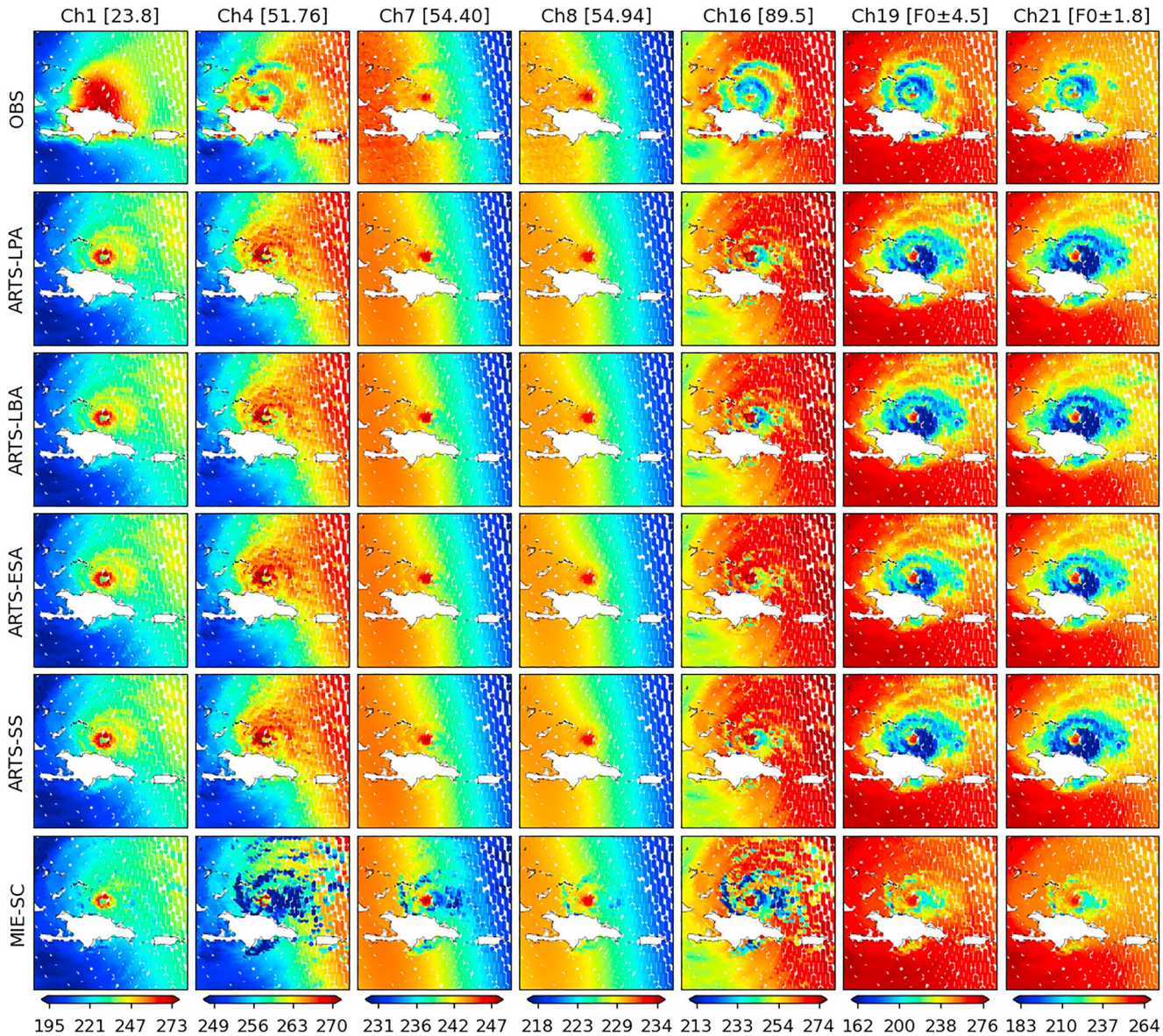

Figure 8. ATMS observed versus CRTM simulated Tbs for Hurricane Irma, 7 September 2017 at 18 UTC, using IFS as input and different CRTM lookup tables. The simulations were conducted using all cloud water content variables provided in IFS and default CRTM/ARTS habits for all cloud types, except varying the habit used for large scale snow water content. The first row in top panel shows ATMS observations and all other rows show simulations performed using CRTM with either ARTS or Mie lookup tables. The abbreviations for habits are included in Table 1. The ATMS channel numbers are printed on the top of each column and the frequency of each channel is given within the brackets in GHz (F0 is equal to 183.31 GHz). All the colorbars have a unit of Kelvin.

channels sensitive to frozen hydrometeors have a significant contribution from mid troposphere. Further analysis showed that the temperature dependency is very similar among the habits, but the PSD dependency largely depends on the habit selected to prescribe the snow water content in the simulations. For instance, the results for GemSnow showed little dependency on the choice of PSD and only for frequencies above 200 GHz.

6.5. Simulated Versus Observed ATMS Measurements

Figure 8 shows the CRTM simulated brightness temperatures using DDA and Mie cloud coefficients versus ATMS observed values over the rainbands of Hurricane Irma on 7 September 2017 at 18:00 UTC. Similar to what we explained in Section 6.3, the cloud water content values were assigned to corresponding default CRTM/ARTS habits, except for alternating the large-scale snow water content among different ARTS habits suitable for

snow clouds. The habits shown in Figure 8 include `LargePlateAggregate`, `LargeBlockAggregate`, `EvansSnowAggregate`, and `SectorSnowflake`. All the simulations were performed using the ARTS lookup tables, except the last row (`MIE-SC`) that used `SNOW_CLOUD` from the Mie lookup tables. The ARTS DDA simulations for channels 1–8 largely perform better than the Mie simulations. As mentioned before, the weighting functions for some of the ATMS temperature sounding channels (channels 9–15) peak mostly above the clouds, therefore the brightness temperatures become less and less sensitive to clouds so that the results of both Mie and DDA become very similar (not shown).

The Mie lookup tables generate excessive scattering for channels 1–8 and 16, but not enough scattering for the water vapor channels. In the specific case of Hurricane Irma, the ARTS lookup tables do not generate enough scattering for channel 16, but the ARTS results are much more consistent with observations for water vapor channels than for channel 16. The simulations for `LargePlateAggregate` and `SectorSnowflake` look visually similar and closer to the ATMS observations than the simulations performed using `EvansSnowAggregate`. These results are consistent with Geer and Baordo (2014) who performed a similar study using RTTOV model and reported much larger negative biases for Mie simulations than for the DDA simulations at 37 GHz. This was attributed to the excessive scattering from frozen hydrometeors in the Mie simulations. They also reported that Mie calculations do not generate enough scattering for upper level ice and snow at 150 GHz (Geer & Baordo, 2014). It should be noted that the choice of the snow habit that yields the best agreement with the observations depends on the NWP model that provides the input atmospheric and cloud profiles. Therefore, this analysis should be repeated for each NWP and data assimilation system.

Although, the data assimilation communities employ statistics such as bias and standard deviation to analyze observed minus simulated values, however as discussed in Geer and Baordo (2014), these statistics lead to so called "double penalty" because the current NWP models cannot predict the clouds in local scales, thus relying on departures can be misleading. Another method that can be used to evaluate the differences between the observed and simulated brightness temperatures is using the frequency distributions. Geer and Baordo (2014) suggested the following statistical parameter, hereafter referred to as histograms discrepancy index (HDI), to evaluate the difference between the frequency distributions (when the bin population is zero, it is set to 0.1 to avoid infinity):

$$G_i = 100\left(\sum_{\text{bins}}\left|\log\frac{\#\text{simulated}}{\#\text{observed}}\right|\right)/\#\text{bins observed} \tag{33}$$

Table 2 shows the HDI values calculated for both the domain of Hurricane Irma and cloudy global observations for some nominal ATMS channels and different CRTM cloud coefficient tables. Since there is no difference between the CRTM simulations for the clear-sky scenes, we have only used the profiles where vertically integrated cloud water content was greater than zero to calculate the HDI. Lower values implies better agreement between simulated and observed values. The DDA database substantially outperforms the Mie database for channels 1–9 over both the domain of Irma and globally, except for channel 7 over the domain of Irma where Mie results are slightly better than the DDA results. These channels are mostly sensitive to water and rain clouds. The difference between the DDA and Mie lookup tables is larger over the domain of Irma than the global domain. This is because of the presence of deep convective clouds over the rainbands of Irma where the DDA performs much better than Mie, however fewer observations are affected by the convective clouds over the global domain relative to the total number of cloudy scenes.

The weighting functions for temperature sounding channels (channel 9–15) generally peak above the clouds so these channels only in specific cases where clouds can reach upper troposphere may be impacted by clouds. Since the convective clouds induced by tropical cyclone can reach upper levels of troposphere, channels like 9 and 10 still show some sensitivity to upper level clouds. Therefore, there is no statistical difference between the DDA and Mie lookup tables for channel 9 in a global domain, but the DDA simulations are still in a better agreement with the observations than the Mie simulations over the domain of Irma. Channel 11 of ATMS is relatively insensitive to clouds so both the DDA and Mie lookup tables perform the same for this channel. The same conclusion applies to channels 12–15 (not shown). The Mie simulations are more consistent with the observations from the ATMS channel 16 (88.2 GHz) than the DDA simulations especially over the rainbands of Hurricane Irma. However, the DDA simulations are in a better agreement with the observations for channels 17 (165.5 GHz) and up which are sensitive to water vapor and frozen clouds.

Table 2
Difference Between Observed and Simulated Values Calculated Using the Statistical Parameter Suggested in Geer and Baordo (2014) to Compare the Histograms

Chan Num	1	2	3	4	5	7	9	11	16	17	18	19	20	21	22	Sum
Chan Freq	23.8	31.4	50.3	51.76	52.8	54.4	55.5	f11	88.2	165.5	f0±7	f0±4.5	f0±3	f0±1.8	f0±1	
ARTS-PT1	41	65	24	23	59	42	34	49	48	29	28	31	35	36	41	583
ARTS-CT1	41	53	24	21	66	40	34	49	49	30	29	28	37	35	41	578
ARTS-SBR	41	54	22	23	65	40	34	49	54	31	28	30	34	34	38	578
ARTS-P4BR	41	53	22	21	66	40	34	49	56	32	24	29	32	35	38	574
ARTS-F3BR	41	52	21	21	67	40	34	49	56	32	25	28	32	36	38	573
ARTS-ICI	41	52	23	24	64	42	34	49	50	28	28	32	34	37	43	583
ARTS-SS	41	53	23	23	67	40	34	49	49	28	28	28	34	37	41	574
ARTS-ESA	42	51	19	24	74	41	34	49	62	39	32	29	33	38	37	604
ARTS-ECA	44	52	24	23	62	42	33	49	47	31	26	30	35	39	44	579
ARTS-LPA	41	54	22	24	66	40	34	49	49	31	27	28	35	35	42	577
ARTS-LCA	41	52	21	21	69	40	34	49	59	37	25	28	32	39	37	585
ARTS-LBA	41	54	22	22	57	42	34	49	47	30	31	34	35	42	47	586
ARTS-ISN	41	53	23	23	67	40	34	49	52	31	28	29	34	34	41	578
MIE-SC	66	88	46	30	65	38	39	49	38	58	57	55	49	47	48	772
ARTS-PT1	23	64	20	23	20	14	13	12	20	26	21	22	25	31	33	368
ARTS-CT1	24	52	19	22	19	14	13	12	21	28	21	21	28	33	31	356
ARTS-SBR	24	52	19	22	18	14	13	12	21	34	24	24	27	30	31	364
ARTS-P4BR	24	52	19	23	19	14	13	12	21	34	21	24	29	29	32	364
ARTS-F3BR	24	52	18	23	20	14	13	12	21	33	21	22	27	29	29	358
ARTS-ICI	23	55	19	22	21	15	13	12	20	25	22	24	27	29	35	362
ARTS-SS	24	52	19	22	19	14	13	12	21	27	19	21	29	32	32	355
ARTS-ESA	24	52	16	22	18	14	13	12	21	41	28	23	29	32	31	377
ARTS-ECA	23	53	19	22	21	15	13	12	20	27	22	22	29	33	35	366
ARTS-LPA	24	53	19	22	18	14	13	12	21	28	18	23	29	29	31	354
ARTS-LCA	24	52	18	23	19	14	13	12	21	39	23	24	29	33	33	375
ARTS-LBA	23	53	19	23	20	15	13	12	20	25	25	23	30	33	39	373
ARTS-ISN	24	52	19	23	19	14	13	12	21	26	22	24	27	28	30	351
MIE-SC	36	86	30	43	28	16	13	12	19	63	68	66	59	55	53	646

Note. The left column shows the scattering database and particle shapes and the last column shows the sum for all the channels. The abbreviations for habits are included in Table 1. The channel frequencies are given in GHz, f11 is equal to 57.290344 ± 0.217 GHz and f0 is 183.31 GHz. The first group of statistics show the statistics for the domain of Irma with 2524 observations and the second group shows the statistics for the global domain with 26088 observations used to calculate the statistics.

Overall, `Flat3BulletRosette`, `SectorSnowflake`, and `Prependicular4BulleteRosette` perform better than other DDA habits over the domain of Irma and the `EvansSnowAggregate` simulations show the least agreement with the observations especially for channels operating above 90 GHz. These habits are followed by `LargePlateAggregate` and `SixBulleteRosette` in terms of yielding best agreement with the observations. In a global domain, `IconSnow`, `LargePlateAggregate`, and `SectorSnowflake` show the best agreement with the observations. In a global domain, `EvansSnowAggregate`, `LargeBlock-Aggregate`, and `LargeColumnAggregate` yield the least agreement with the ATMS observations. Overall except for a few cases, any DDA habit outperforms the Mie results. Channels below 82 GHz are not substantially impacted by the choice of snow habit especially in a global domain. However, the DDA lookup tables still perform much better than the Mie lookup tables for these channels as well. `PlateType1` shows a relatively large error for channel 2 compared with other habits, but this seems to be due to an artifact in the DDA lookup tables.

The results are consistent with Geer (2021) who reported that `LargePlateAggregate`, and `SectorSnowflake` yield the best agreement with the observations using model profiles from a similar version of the IFS forecast model but with the RTTOV-SCATT radiative transfer model and the tropical PSD of Field et al. (2007) for snow hydrometers. However, our results are not consistent with Fox (2020) who reported that `LargeColumnAggregate` yields the smallest root mean square of the differences between observed and simulated values using atmospheric profiles from a regional model and the F07 tropical PSD. In addition, unlike Fox (2020) who reported poor results for `EightColumnAggregate`, in our analysis `EvansSnowAggregate` yields the least agreement with observations over both global and Irma domains. However, both the input profiles and also the RT model used by Fox (2020) were different from what we have evaluated in this paper. Ekelund, Eriksson, and Pfreundschuh (2020) reported best agreement with GMI observations for `LargeColumnAggregate` and `EvansSnowAggregate`, but `EvansSnowAggregate` yields the least agreement in our analysis over both Irma and global domains. The consistency between Geer (2021) and this study despite the fact that we have used different PSDs and radiative transfer models, CRTM uses a more sophisticated scattering solver (advanced doubling adding) than RTTOV delta-Eddington, show that the input atmospheric and especially cloud water content profiles may still play the major role in the agreement between simulations and observations.

Since both sector snow flake and large plate aggregate perform well over both global and Irma domains, either can be used to define the snow hydrometeors in CRTM. However, we recommend to define snow hydrometeors using `LargePlateAggregate` because `LargePlateAggregate` is a more physically realistic model of snow than the sector snow flake, which is overly smooth for high frequency radiative transfer. More precisely, large plate aggregate has justifiable features on smaller spatial scales, which may not matter at 183 GHz but might well give better results in the sub-mm spectral domain. Also, aggregate models appear to produce better results than pristine crystals for a range of remote measurements including triple-frequency radar signatures (e.g., Tyynela & Von Lerber, 2019) and they reflect the prevalence of aggregates in midlatitude snowfall (e.g., Jiusto & Weickmann, 1973).

7. Conclusions

Radiative transfer models are extensively used for the assimilation of satellite observations into NWP models as well as retrieving geophysical products from satellite measurements. CRTM is a community model developed by NOAA JCSDA and widely used for different purposes requiring RT calculations. CRTM requires bulk scattering lookup tables in order to perform all-sky RT calculations. However, the current lookup tables for MW frequencies were generated based on the Mie theory by assuming spherical frozen particles. The scattering lookup tables generated using the DDA technique has shown to largely improve the RT scattering calculations in the MW region (Geer & Baordo, 2014). We discuss the implementation and validation of a DDA database that was originally developed for the ARTS RT model into CRTM. However, the ARTS database only provides single scattering properties of different habits, while CRTM requires bulk scattering properties. The CRTM cloud coefficients were previously generated based on the effective radius for representing the size of the particles. However, the effective radius is not often included among the output fields by the NWP models, thus need to be estimated from other geophysical variables such as water content. Therefore, in addition to calculating the CRTM bulk scattering properties from the DDA single scattering database, the CRTM was also largely modified to use cloud water content (kg m^{-3}), instead of effective radius, for performing the interpolation over the mass of particles. CRTM already requires water content as input, thus no extra variables are required for performing scattering calculations using the new ARTS DDA database.

Although these results clearly show the advantage of the ARTS database over the Mie dataset, different error sources such as error in the observations, displacement of clouds in the IFS forecast, or errors in the input atmospheric and cloud profiles contribute to the differences between simulated and observed values. Aside from the improvements in the simulations shown throughout the paper, a major advantage of the new dataset is a large number of habits that can be used to tune the data assimilation systems to perform well in different weather conditions. For instance, CRTM simulations conducted using the IFS short term forecast as input show that `Sector Snowflake` and `LargePlateAggregate` overall perform better than other DDA habits. However, similar to Ekelund, Eriksson, and Pfreundschuh (2020) who reported that no conclusive decision can be made in terms of best habit, we also found a large variation in the choice of best habit for different channels and also whether the histogram differences are calculated over the domain of Irma or globally. These recommended habits also likely

depend on the atmospheric and cloud profiles used as input to the RT model. In addition, we selected the best PSD based on the renormalization factor but the results show that the simulated brightness temperatures largely depend on the PSD used to compute the bulk scattering properties. Therefore, we recommend that this analysis should be repeated for each NWP and data assimilation system for a large number of synoptic weather events. Other sources of errors in the RT all-sky calculations that were not investigated in this study include, the accuracy of scattering solvers, the plane parallel approximation, and also ignoring 3D structure of clouds and precipitation in the RT calculations. However, these errors have been the subject of other studies (Barlakas et al., 2022; Hogan & Shonk, 2013; McLinden & Bourassa, 2010). Additionally, some of the advanced optimized scattering solvers implemented into CRTM are expected to have enough accuracy for the assimilation of satellite observations or other general remote sensing applications such as product retrieval (Bennartz & Greenwald, 2011).

Appendix A: ARTS Scattering Parameters

This section includes the extra figures for ARTS single scattering parameters and also CRTM mass scattering parameters computed using the ARTS scattering dataset.

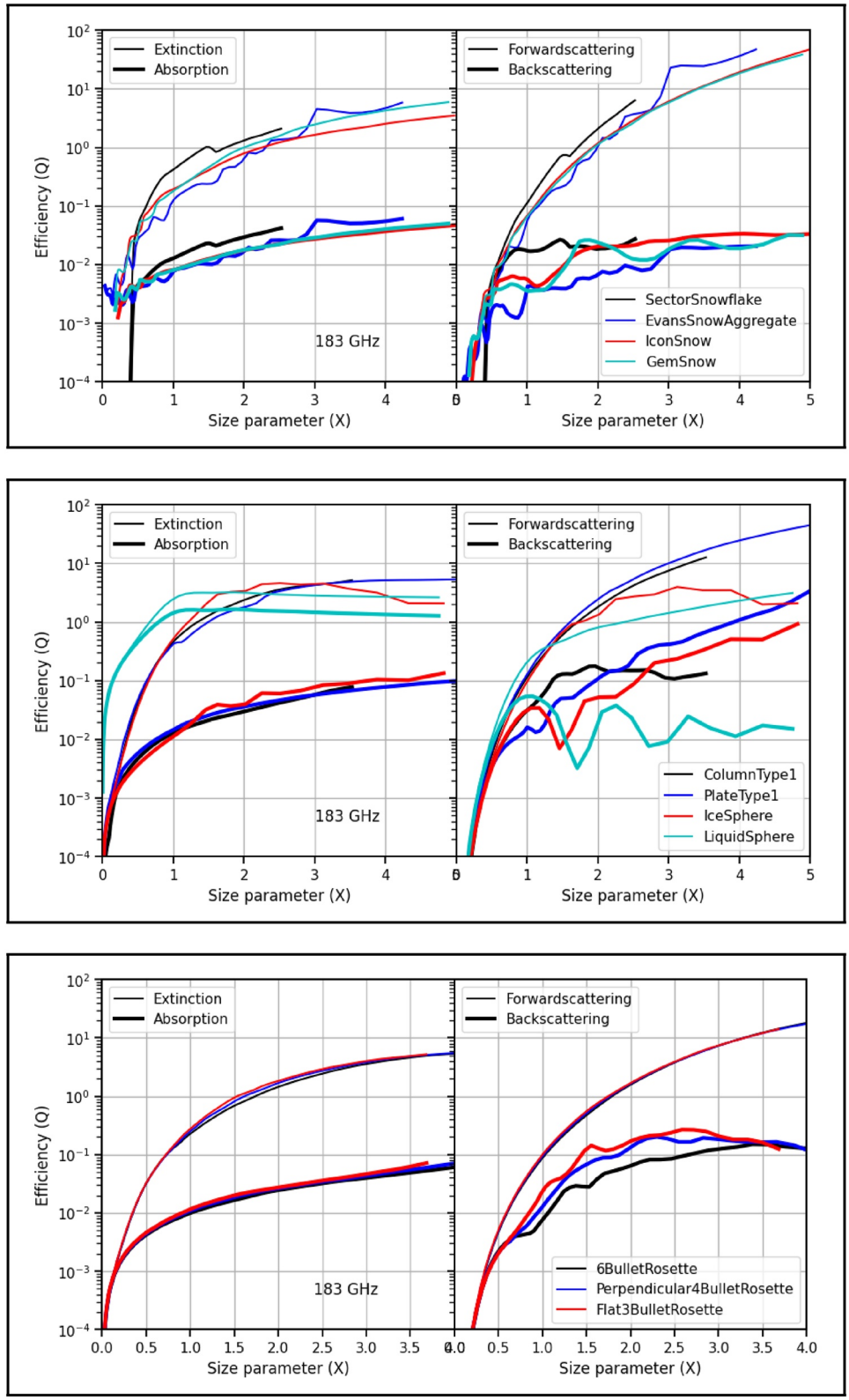

Figure A1. Extinction, absorption, forwardscattering, and backscattering efficiencies for different ARTS habits computed at a frequency of 183 GHz and a temperature of 260 K. Both size parameter (X) and single scattering efficiencies (Q) are unitless.

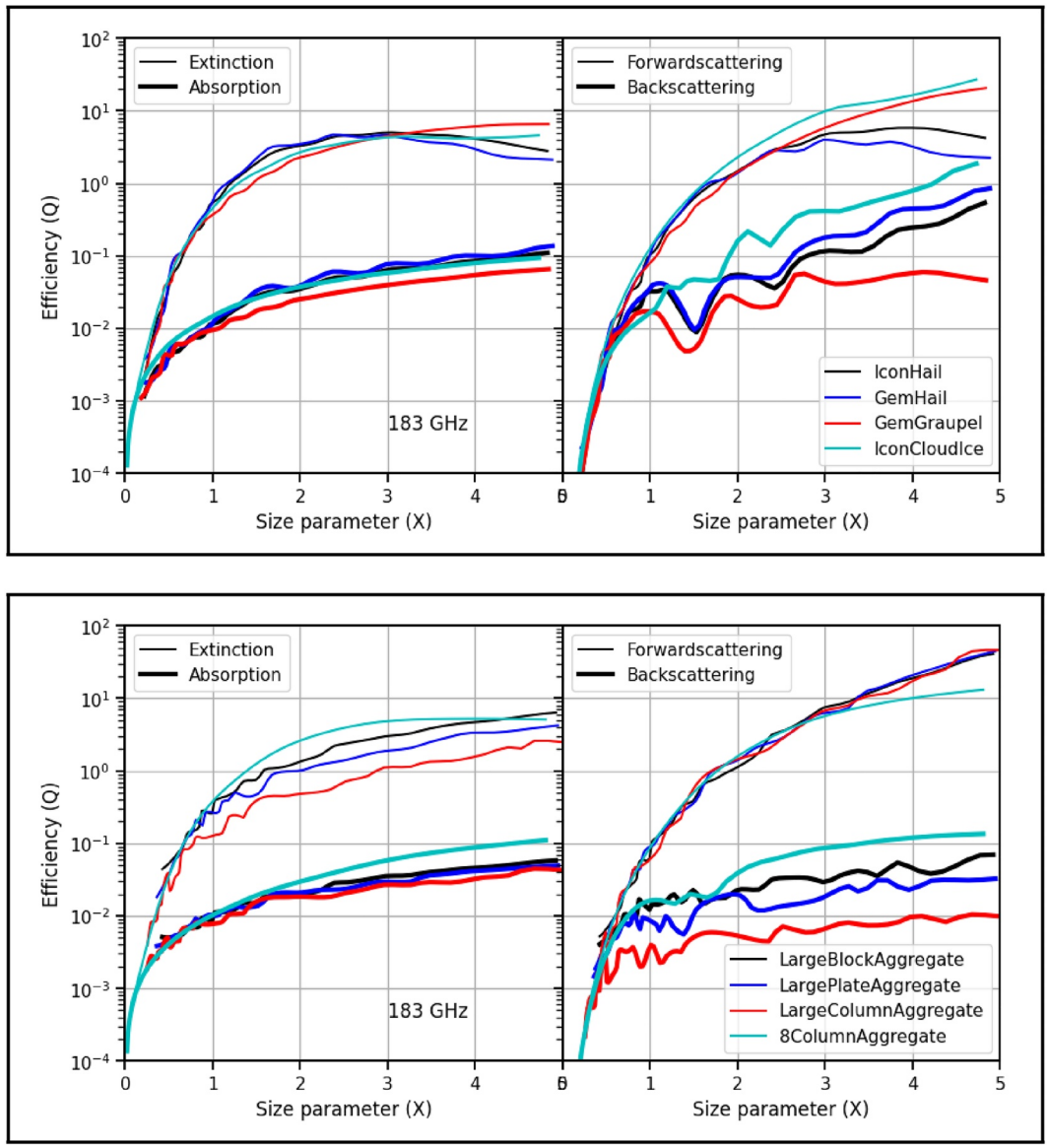

Figure A1. (Continued)

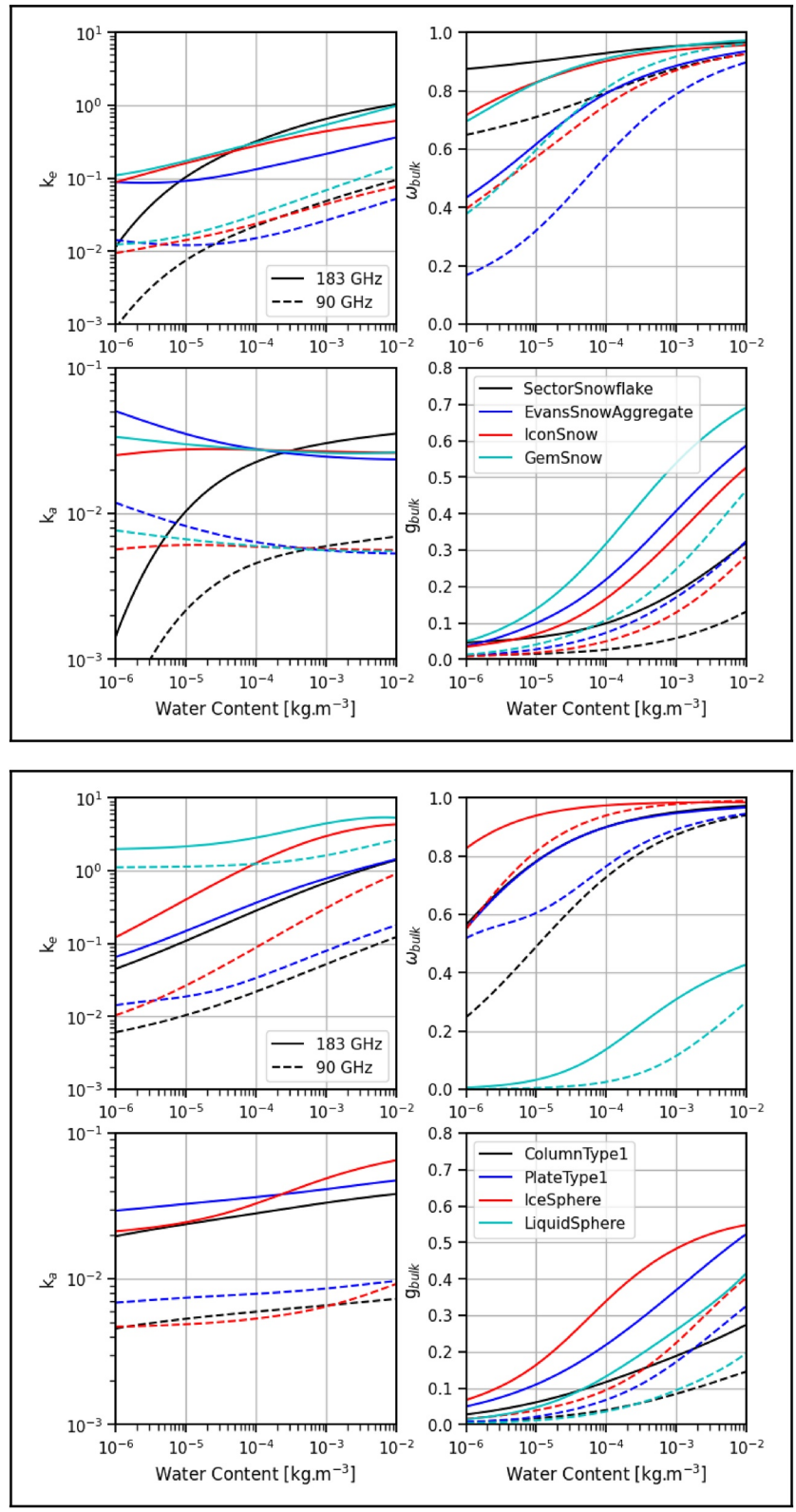

Figure A2. Mass extinction (k_e) and absorption (k_a) coefficients (both in $m^2\ kg^{-1}$) as well as bulk single scattering albedo (ω_{bulk}), and asymmetry parameter (g_{bulk}) (both unitless) for different habits calculated at 260 K. The legends for habits and frequencies are applicable to all the depicts in the same group.

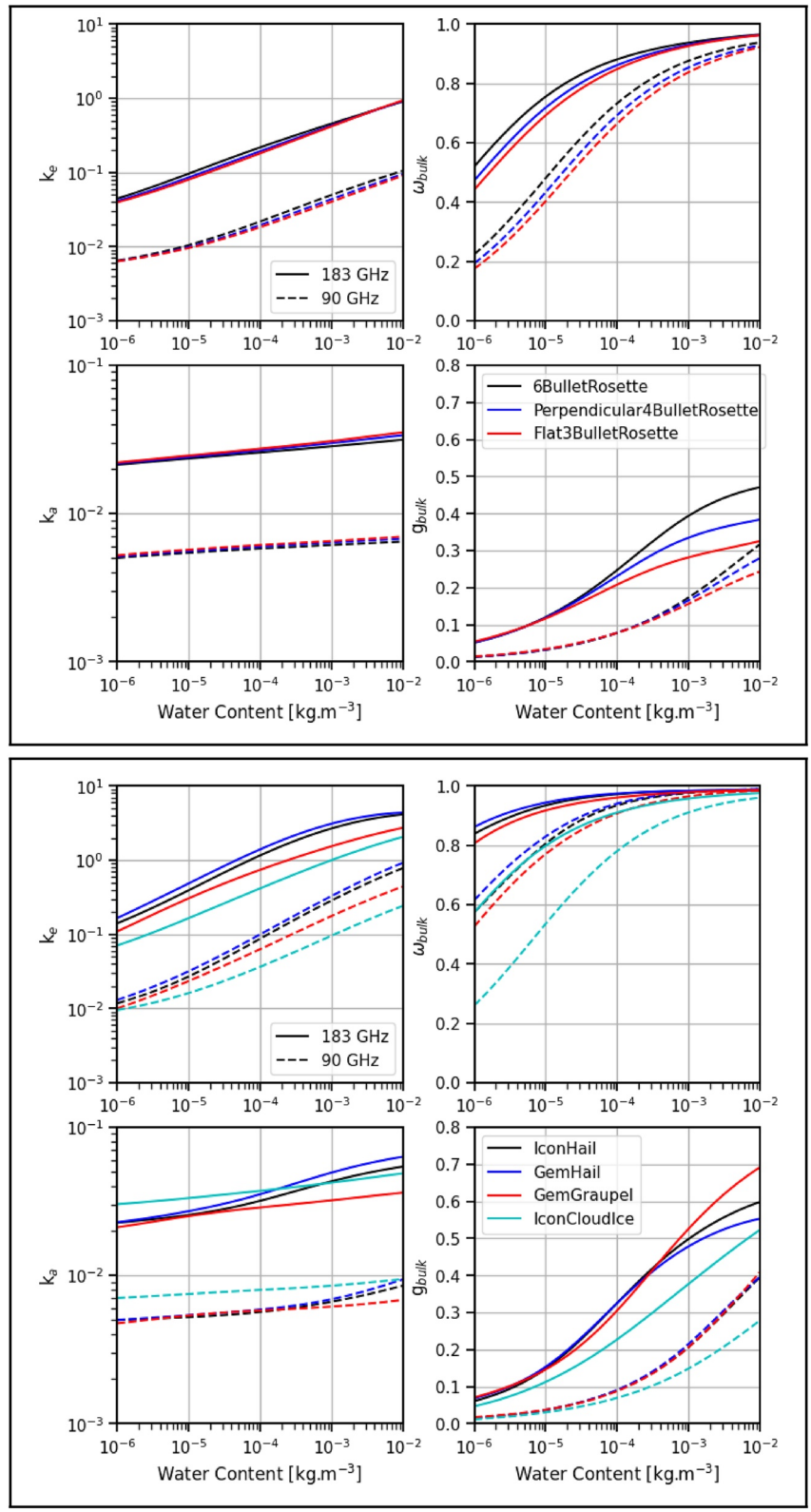

Figure A2. (Continued)

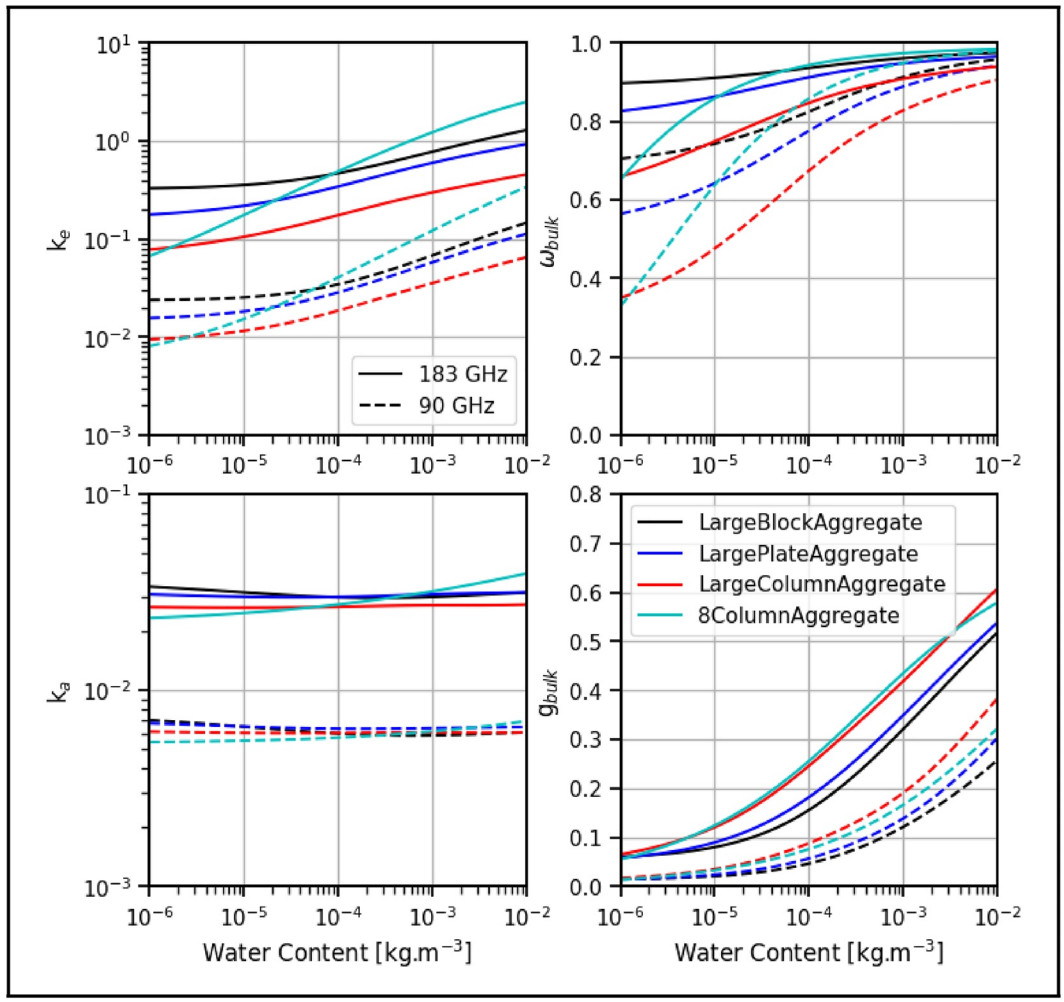

Figure A2. (Continued)

Data Availability Statement

CRTM is a community model publicly available from the JCSDA (Joint Center for Satellite Data Assimilation, 2020). ATMS data are available from NOAA CLASS (National Oceanic and Atmospheric Administration, 2017) and IFS data were provided by Geer (2022). The ARTS single scattering database is also publicly available at Zenodo (Ekelund, Brath, et al., 2020).

Acknowledgments
This study was funded by the NOAA Joint Polar Satellite System (JPSS) program, Grant NA19NES4320002 (Cooperative Institute for Satellite Earth System Studies) and the NASA Modeling, Analysis, and Prediction (MAP) Program Grant 80NSSC21K1361. Thanks to three anonymous reviewers as well as the journal editor for their time and effort to review the paper.

References

Abel, S. J., & Boutle, I. A. (2012). An improved representation of the raindrop size distribution for single-moment microphysics schemes. *Quarterly Journal of the Royal Meteorological Society*, *138*(669), 2151–2162. https://doi.org/10.1002/qj.1949

Baordo, F., & Geer, A. J. (2016). Assimilation of SSMIS humidity-sounding channels in all-sky conditions over land using a dynamic emissivity retrieval. *Quarterly Journal of the Royal Meteorological Society*, *142*(700), 2854–2866. https://doi.org/10.1002/qj.2873

Barlakas, V., Galligani, V. S., Geer, A. J., & Eriksson, P. (2022). On the accuracy of RTTOV-SCATT for radiative transfer at all-sky microwave and submillimeter frequencies. *Journal of Quantitative Spectroscopy and Radiative Transfer*, *283*, 108137. https://doi.org/10.1016/j.jqsrt.2022.108137

Barton, N., Metzger, E. J., Reynolds, C. A., Ruston, B., Rowley, C., Smedstad, O. M., et al. (2021). The navy's Earth system prediction capability: A new global coupled atmosphere-ocean-sea ice prediction system designed for daily to subseasonal forecasting. *Earth and Space Science*, *8*(4), e2020EA001199. https://doi.org/10.1029/2020EA001199

Bauer, P., Moreau, E., Chevallier, F., & O'keeffe, U. (2006). Multiple-scattering microwave radiative transfer for data assimilation applications. *Quarterly Journal of the Royal Meteorological Society*, *132*(617), 1259–1281. https://doi.org/10.1256/qj.05.153

Bennartz, R., & Greenwald, T. (2011). Current problems in scattering radiative transfer modelling for data assimilation. *Quarterly Journal of the Royal Meteorological Society*, *137*(661), 1952–1962. https://doi.org/10.1002/qj.953

Boukabara, S.-A., Garrett, K., Chen, W., Iturbide-Sanchez, F., Grassotti, C., Kongoli, C., et al. (2011). Mirs: An all-weather 1dvar satellite data assimilation and retrieval system. *IEEE Transactions on Geoscience and Remote Sensing*, *49*(9), 3249–3272. https://doi.org/10.1109/tgrs.2011.2158438

Boukabara, S.-A., Moradi, I., Atlas, R., Casey, S. P. F., Cucurull, L., Hoffman, R. N., et al. (2016). Community global observing system simulation experiment (osse) package (cgop): Description and usage. *Journal of Atmospheric and Oceanic Technology*, *33*(8), 1759–1777. https://doi.org/10.1175/jtech-d-16-0012.1

Brath, M., Ekelund, R., Eriksson, P., Lemke, O., & Buehler, S. A. (2020). Microwave and submillimeter wave scattering of oriented ice particles. *Atmospheric Measurement Techniques*, *13*(5), 2309–2333. https://doi.org/10.5194/amt-13-2309-2020

Chandrasekhar, S. (2011). *Radiative transfer*. Dover Publications.

DeVoe, H. (1964). Optical properties of molecular aggregates. I. Classical model of electronic absorption and refraction. *The Journal of Chemical Physics*, *41*(2), 393–400. https://doi.org/10.1063/1.1725879

Ding, J., Bi, L., Yang, P., Kattawar, G. W., Weng, F., Liu, Q., & Greenwald, T. (2017). Single-scattering properties of ice particles in the microwave regime: Temperature effect on the ice refractive index with implications in remote sensing. *Journal of Quantitative Spectroscopy and Radiative Transfer*, *190*, 26–37. https://doi.org/10.1016/j.jqsrt.2016.11.026

Draine, B. T., & Flatau, P. J. (1994). Discrete-dipole approximation for scattering calculations. *Josa A*, *11*(4), 1491–1499. https://doi.org/10.1364/josaa.11.001491

Draine, B. T., & Flatau, P. J. (2000). User guide for the discrete dipole approximation code DDSCAT (Version 5a10). arXiv:astro-ph/0008151.

Duncan, D. I., Bormann, N., Geer, A. J., & Weston, P. (2022). Assimilation of amsu-a in all-sky conditions. *Monthly Weather Review*, *150*(5), 1023–1041. https://doi.org/10.1175/mwr-d-21-0273.1

Ekelund, R., Brath, M., Mendrok, J., & Eriksson, P. (2020). Arts microwave single scattering properties database dataset. *Zenodo*. https://doi.org/10.5281/zenodo.4646605

Ekelund, R., Eriksson, P., & Kahnert, M. (2020). Microwave single-scattering properties of non-spheroidal raindrops. *Atmospheric Measurement Techniques*, *13*(12), 6933–6944. https://doi.org/10.5194/amt-13-6933-2020

Ekelund, R., Eriksson, P., & Pfreundschuh, S. (2020). Using passive and active observations at microwave and sub-millimetre wavelengths to constrain ice particle models. *Atmospheric Measurement Techniques*, *13*(2), 501–520. https://doi.org/10.5194/amt-13-501-2020

Eriksson, P., Ekelund, R., Mendrok, J., Brath, M., Lemke, O., & Buehler, S. A. (2018). A general database of hydrometeor single scattering properties at microwave and sub-millimetre wavelengths. *Earth System Science Data*, *10*(3), 1301–1326. https://doi.org/10.5194/essd-10-1301-2018

Eriksson, P., Jamali, M., Mendrok, J., & Buehler, S. A. (2015). On the microwave optical properties of randomly oriented ice hydrometeors. *Atmospheric Measurement Techniques*, *8*(5), 1913–1933. https://doi.org/10.5194/amt-8-1913-2015

Field, P. R., Heymsfield, A. J., & Bansemer, A. (2007). Snow size distribution parameterization for midlatitude and tropical ice clouds. *Journal of the Atmospheric Sciences*, *64*(12), 4346–4365. https://doi.org/10.1175/2007jas2344.1

Field, P. R., Heymsfield, A. J., Detwiler, A. G., & Wilkinson, J. M. (2019). Normalized hail particle size distributions from the T-28 storm-penetrating aircraft. *Journal of Applied Meteorology and Climatology*, *58*(2), 231–245. https://doi.org/10.1175/jamc-d-18-0118.1

Field, P. R., Hogan, R. J., Brown, P. R. A., Illingworth, A. J., Choularton, T. W., & Cotton, R. J. (2005). Parametrization of ice-particle size distributions for mid-latitude stratiform cloud. *Quarterly Journal of the Royal Meteorological Society*, *131*(609), 1997–2017. https://doi.org/10.1256/qj.04.134

Fox, S. (2020). An evaluation of radiative transfer simulations of cloudy scenes from a numerical weather prediction model at sub-millimetre frequencies using airborne observations. *Remote Sensing*, *12*(17), 2758. https://doi.org/10.3390/rs12172758

Fritsch, F. N., & Butland, J. (1984). A method for constructing local monotone piecewise cubic interpolants. *SIAM Journal on Scientific and Statistical Computing*, *5*(2), 300–304. https://doi.org/10.1137/0905021

Geer, A. J. (2021). Physical characteristics of frozen hydrometeors inferred with parameter estimation. *Atmospheric Measurement Techniques*, *14*(8), 5369–5395. https://doi.org/10.5194/amt-14-5369-2021

Geer, A. J. (2022). Model profiles at satellite locations, 09-21 UTC, 7th September, 2017. Dataset. *Zenodo*. https://doi.org/10.5281/zenodo.6362200

Geer, A. J., & Baordo, F. (2014). Improved scattering radiative transfer for frozen hydrometeors at microwave frequencies. *Atmospheric Measurement Techniques*, *7*(6), 1839–1860. https://doi.org/10.5194/amt-7-1839-2014

Geer, A. J., & Bauer, P. (2011). Observation errors in all-sky data assimilation. *Quarterly Journal of the Royal Meteorological Society*, *137*(661), 2024–2037. https://doi.org/10.1002/qj.830

Geer, A. J., Bauer, P., Lonitz, K., Barlakas, V., Eriksson, P., Mendrok, J., et al. (2021). Bulk hydrometeor optical properties for microwave and sub-mm radiative transfer in RTTOV-SCATT v13.0. *Geoscientific Model Development Discussions*, 1–45. https://doi.org/10.5194/gmd-2021-73

Gelaro, R., McCarty, W., Suá rez, M. J., Todling, R., Molod, A., Takacs, L., et al. (2017). The modern-era retrospective analysis for research and applications, version 2 (merra-2). *Journal of Climate*, *30*(14), 5419–5454. https://doi.org/10.1175/jcli-d-16-0758.1

Goldberg, M., Kilcoyne, H., Cikanek, H., & Mehta, A. (2013). Joint polar satellite system: The United States next generation civilian polar-orbiting environmental satellite system. *Journal of Geophysical Research: Atmospheres*, *118*(24), 13463–13475. https://doi.org/10.1002/2013jd020389

Heidinger, A. K., O'Dell, C., Bennartz, R., & Greenwald, T. (2006). The successive-order-of-interaction radiative transfer model. Part I: Model development. *Journal of Applied Meteorology and Climatology*, *45*(10), 1388–1402. https://doi.org/10.1175/jam2387.1

Hogan, R. J., & Shonk, J. K. P. (2013). Incorporating the effects of 3D radiative transfer in the presence of clouds into two-stream multilayer radiation schemes. *Journal of the Atmospheric Sciences*, *70*(2), 708–724. https://doi.org/10.1175/jas-d-12-041.1

Hong, G. (2007). Parameterization of scattering and absorption properties of nonspherical ice crystals at microwave frequencies. *Journal of Geophysical Research*, *112*(D11), D11208. https://doi.org/10.1029/2006jd008364

Hong, G., Yang, P., Baum, B. A., Heymsfield, A. J., Weng, F., Liu, Q., et al. (2009). Scattering database in the millimeter and submillimeter wave range of 100-1000 GHz for nonspherical ice particles. *Journal of Geophysical Research*, *114*(D6), D06201. https://doi.org/10.1029/2008jd010451

Jiusto, J. E., & Weickmann, H. K. (1973). Types of snowfall. *Bulletin of the American Meteorological Society*, *54*(11), 1148–1162. https://doi.org/10.1175/1520-0477(1973)054<1148:tos>2.0.co;2

Joint Center for Satellite Data Assimilation. (2020). Community radiative transfer model. *Software*. Retrieved from https://www.jcsda.org/crtm

Kim, E., Lyu, C.-H. J., Anderson, K., Vincent Leslie, R., & Blackwell, W. J. (2014). S-npp atms instrument prelaunch and on-orbit performance evaluation. *Journal of Geophysical Research: Atmospheres*, *119*(9), 5653–5670. https://doi.org/10.1002/2013jd020483

Kim, M., Jin, J., Akkraoui, A. E., McCarty, W., Todling, R., Gu, W., & Gelaro, R. (2020). The framework for assimilating all-sky GPM microwave imager brightness temperature data in the NASA GEOS data assimilation system. *Monthly Weather Review*, *148*(6), 2433–2455. https://doi.org/10.1175/mwr-d-19-0100.1

Liou, K. N. (2002). *An introduction to atmospheric radiation*. Academic Press.

Liu, G. (2004). Approximation of single scattering properties of ice and snow particles for high microwave frequencies. *Journal of the Atmospheric Sciences*, *61*(20), 2441–2456. https://doi.org/10.1175/1520-0469(2004)061<2441:aosspo>2.0.co;2

Liu, G. (2008). A database of microwave single-scattering properties for nonspherical ice particles. *Bulletin of the American Meteorological Society*, *89*(10), 1563–1570. https://doi.org/10.1175/2008bams2486.1

Liu, Q., Liu, X., Chen, Y., Nalli, N. R., & Tan, C. (2018). 7.07 - fast radiative transfer algorithms for real-time sounder applications. In S. Liang (Ed.), *Comprehensive remote sensing* (pp. 197–234). Elsevier. https://doi.org/10.1016/b978-0-12-409548-9.10391-4

Liu, Q., & Weng, F. (2006). Advanced doubling-adding method for radiative transfer in planetary atmospheres. *Journal of the Atmospheric Sciences*, *63*(12), 3459–3465. https://doi.org/10.1175/jas3808.1

Liu, Q., Weng, F., Han, Y., & Van Delst, P. (2008). Community radiative transfer model for scattering transfer and applications. *Igarss 2008 - 2008 IEEE International Geoscience and Remote Sensing Symposium*, *4*, 1193–1196. https://doi.org/10.1109/igarss.2008.4779942

McCarty, W., Carvalho, D., Moradi, I., & Privé, N. C. (2021). Observing system simulation experiments investigating atmospheric motion vectors and radiances from a constellation of 4-5-μm infrared sounders. *Journal of Atmospheric and Oceanic Technology*, *38*(2), 331–347. https://doi.org/10.1175/jtech-d-20-0109.1

McFarquhar, G. M., & Heymsfield, A. J. (1997). Parameterization of tropical cirrus ice crystal size distributions and implications for radiative transfer: Results from CEPEX. *Journal of the Atmospheric Sciences*, *54*(17), 2187–2200. https://doi.org/10.1175/1520-0469(1997)054<2187:potcic>2.0.co;2;2

McLinden, C. A., & Bourassa, A. E. (2010). A systematic error in plane-parallel radiative transfer calculations. *Journal of the Atmospheric Sciences*, *67*(5), 1695–1699. https://doi.org/10.1175/2009jas3322.1

Moradi, I., Evans, F., McCarty, W., Cordero-Fuentes, M., Gelaro, R., & Black, R. (2020). Assimilation of satellite microwave observations over the rainbands of tropical cyclones. *Monthly Weather Review*, *148*(12), 4729–4745. https://doi.org/10.1175/mwr-d-19-0341.1

Moradi, I., Ferraro, R., Eriksson, P., & Weng, F. (2015). Intercalibration and validation of observations from atms and saphir microwave sounders. *IEEE Transactions on Geoscience and Remote Sensing*, *53*(11), 5915–5925. https://doi.org/10.1109/tgrs.2015.2427165

Moradi, I., Goldberg, M., Brath, M., Ferraro, R., Buehler, S. A., Saunders, R., & Sun, N. (2020). Performance of radiative transfer models in the microwave region. *Journal of Geophysical Research: Atmospheres*, *125*(6), e2019JD031831. https://doi.org/10.1029/2019jd031831

National Oceanic and Atmospheric Administration. (2017). The comprehensive large array-data stewardship system (CLASS). [Dataset]. Retrieved from https://www.class.noaa.gov

Penttilä, A., Zubko, E., Lumme, K., Muinonen, K., Yurkin, M. A., Draine, B., et al. (2007). Comparison between discrete dipole implementations and exact techniques. *Journal of Quantitative Spectroscopy and Radiative Transfer*, *106*(1), 417–436. https://doi.org/10.1016/j.jqsrt.2007.01.026

Sieron, S. B., Clothiaux, E. E., Zhang, F., Lu, Y., & Otkin, J. A. (2017). Comparison of using distribution-specific versus effective radius methods for hydrometeor single-scattering properties for all-sky microwave satellite radiance simulations with different microphysics parameterization schemes. *Journal of Geophysical Research: Atmospheres*, *122*(13), 7027–7046. https://doi.org/10.1002/2017jd026494

Stamnes, K., Tsay, S.-C., Wiscombe, W., & Jayaweera, K. (1988). Numerically stable algorithm for discrete-ordinate-method radiative transfer in multiple scattering and emitting layered media. *Applied Optics*, *27*(12), 2502–2509. https://doi.org/10.1364/ao.27.002502

Stegmann, P. G., Tang, G., Yang, P., & Johnson, B. T. (2018). A stochastic model for density-dependent microwave Snow- and Graupel scattering coefficients of the NOAA JCSDA community radiative transfer model. *Journal of Quantitative Spectroscopy and Radiative Transfer*, *211*, 9–24. https://doi.org/10.1016/j.jqsrt.2018.02.026

Tong, M., Zhu, Y., Zhou, L., Liu, E., Chen, M., Liu, Q., & Lin, S.-J. (2020). Multiple hydrometeors all-sky microwave radiance assimilation in fv3gfs. *Monthly Weather Review*, *148*(7), 2971–2995. https://doi.org/10.1175/mwr-d-19-0231.1

Tyynela, J., & Von Lerber, A. (2019). Validation of microphysical snow models using in situ, multifrequency, and dual-polarization radar measurements in Finland. *Journal of Geophysical Research: Atmospheres*, *124*(23), 13273–13290. https://doi.org/10.1029/2019JD030721

Weng, F., Zou, X., Sun, N., Yang, H., Tian, M., Blackwell, W. J., et al. (2013). Calibration of suomi national polar-orbiting partnership advanced technology microwave sounder. *Journal of Geophysical Research: Atmospheres*, *118*(19), 11187–11200. https://doi.org/10.1002/jgrd.50840

Yurkin, M. A., & Hoekstra, A. G. (2007). The discrete dipole approximation: An overview and recent developments. *Journal of Quantitative Spectroscopy and Radiative Transfer*, *106*(1), 558–589. https://doi.org/10.1016/j.jqsrt.2007.01.034

Yurkin, M. A., & Hoekstra, A. G. (2011). The discrete-dipole-approximation code ADDA: Capabilities and known limitations. *Journal of Quantitative Spectroscopy and Radiative Transfer*, *112*(13), 2234–2247. https://doi.org/10.1016/j.jqsrt.2011.01.031

Zhou, L., Harris, L., Chen, J.-H., Gao, K., Guo, H., Xiang, B., et al. (2022). Improving global weather prediction in gfdl shield through an upgraded gfdl cloud microphysics scheme. *Journal of Advances in Modeling Earth Systems*, *14*(7), e2021MS002971. https://doi.org/10.1029/2021MS002971

Zhu, Y., Derber, J. C., Purser, R. J., Ballish, B. A., & Whiting, J. (2015). Variational correction of aircraft temperature bias in the NCEP's GSI analysis system. *Monthly Weather Review*, *143*(9), 3774–3803. https://doi.org/10.1175/mwr-d-14-00235.1